Stress focusing in elastic sheets

T. A. Witten*

James Franck Institute. University of Chicago, 929 E. 57th Street, Chicago IL 60637

We review recent progress in understanding phenomena like crumpling, in which elastic membranes or sheets subject to structureless forces develop sharply curved structure over a small fraction of their surface. In the limit of zero thickness these structures become singular. After reviewing several related phenomena we note the physical elements that give rise to the singular behavior: elasticity and the nearly inextensible behavior of thin sheets. This singular behavior has counterparts in higher dimensions. Then we discuss the most basic of these singularities, the vertex. We describe mathematical progress in describing the d-cone, a simple realization of a vertex. We concentrate on the size of the core that governs the departure from singularity and conclude that fundamental understanding is lacking. We point out further mysterious behavior at the region where a d-cone is supported. We then discuss an emergent singularity that appears when two or more vertices are present: the stretching ridge. We offer several accounts of the scale of this singularity from qualitative scaling arguments to a formal asymptotic analysis. We discuss recent experiments and theories about the interaction of ridges and vertices and review the evidence that these ridges dominate the mechanics of crumpled sheets.

Typeset May 15, 2007. For errata see http://panza.uchicago.edu/RMP/

Contents

I. Introduction 3
- A. history 4
- B. interface focusing 5
- C. prospectus 6

II. Basic energies and isometry 7
- A. elastic energies 7
- B. isometric distortions 9
- C. higher dimensions 10
  1. stretching vertices 13
  2. ridges 14

III. D-cones 15
- A. kinematics 16
- B. mechanics 17
- C. core region 19
- D. d-cone experiments and numerics 20
  1. unexpected features 21

IV. Stretching ridge structures 22
- A. variants 22
- B. scaling of ridge width 23
- C. generalization 25
- D. implications 26
- E. amplitude dependence 26
- F. ring ridge 27

V. The minimal ridge 27
- A. Föppl–von Karman equations 27
- B. dimensional simplification 29
- C. boundary conditions for minimal ridge 29
- D. ridge shape 30
- E. ridge-to-vertex crossover 31
- F. amplitude scaling 31
- G. far field 31
- H. d-cones revisited 31

*Electronic address: t-witten@uchicago.edu

VI. Ridge simulations and experiments 32
A. numerical methods 32
B. main scaling predictions 32
C. unpredicted features 33
D. higher dimensions 34

VII. Interacting vertices and ridges 35
A. vertex interactions 36
B. ridge interactions 36
C. ridge buckling 36
D. crushing energy 37
E. heterogeneity and complexity. 38

VIII. Conclusion 38

Acknowledgments 39

References 39

Appendix: ridge-to-vertex crossover 41

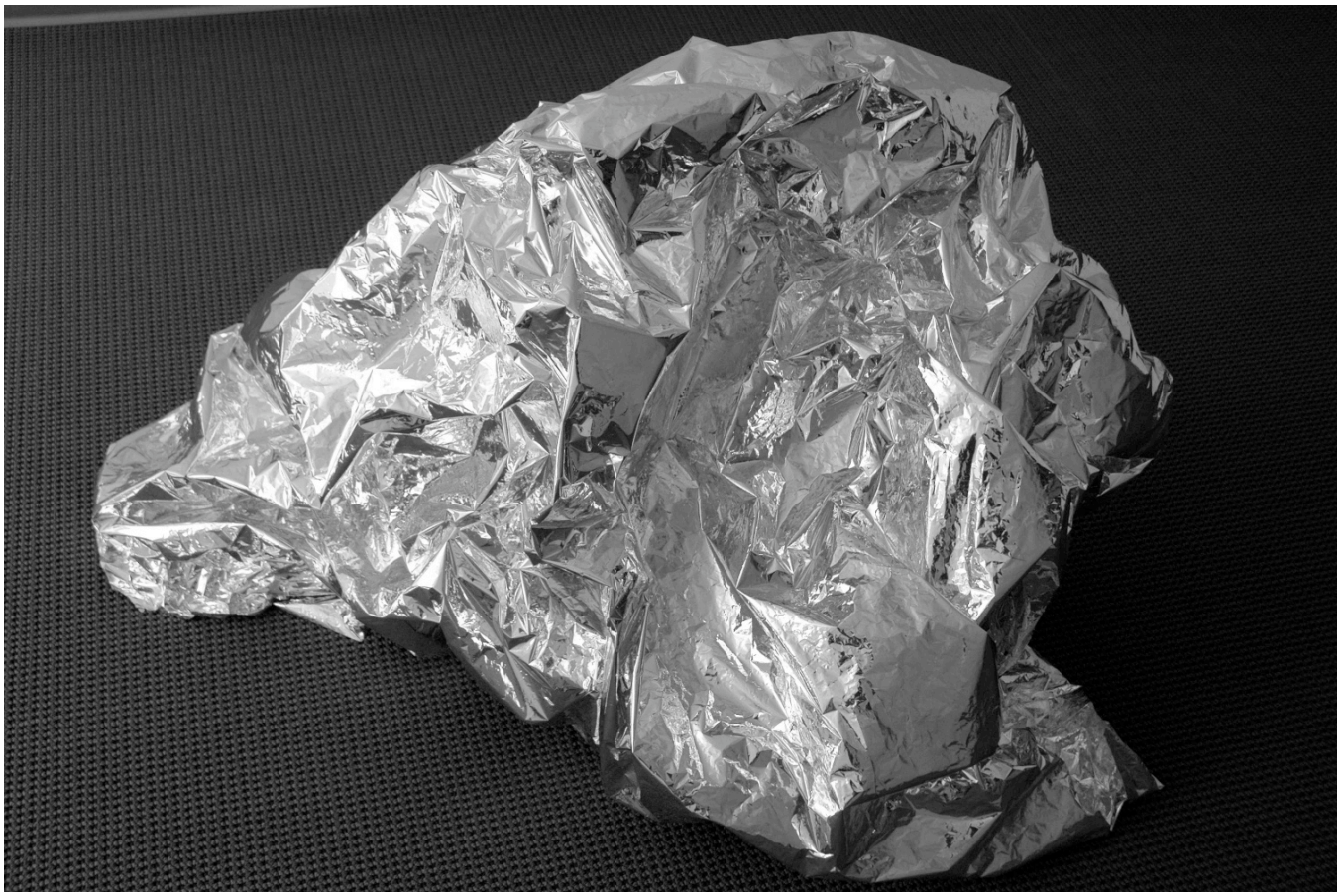

FIG. 1 A loosely crumpled sheet of aluminized mylar, 2 meters in width and 10 microns in thickness, courtesy of Henry Frisch

I. INTRODUCTION

Imagine a piece of paper inside a large spherical container. Then imagine shrinking the container, so that the paper inside must deform. The paper develops sharp points and bends: it *crumples*. No such sharpness appears if one confines a thin wire or thread in the same sphere. These one-dimensional objects curl up uniformly as they are confined, with none of the sharp structure seen in the paper. This review explores the origin and nature of these sharp features that appear when a two-dimensional solid sheet or membrane is confined, as in Figure 1.

The sharp structure of crumpling is a form of energy focusing. As the sphere begins to shrink, the elastic energy of deformation, initially smoothly distributed, becomes more and more nonuniform. It becomes concentrated in the strongly bent regions. This concentration grows more and more pronounced if one repeats the experiment with thinner and thinner sheets. Such spontaneous focusing of energy has been an important preoccupation of physics throughout the 20th century. A classical example is strong turbulence (Nelkin , 1992), in which kinetic energy uniformly injected into a fluid becomes progressively concentrated into regions of strong vorticity in space, and strong intermittency in time. Strong vibrational excitations in a medium lead to focusing into shock waves (Robey *et al.* , 2002). Strong mechanical forcing of solids leads to fracture: uniform perturbation creates a focused response (DeArcangelis *et al.* , 1989). Dielectric breakdown of a solid under a uniform electric field is an analogous phenomenon (Gyure, Beale , 1992) . Such focusing is paradoxical. Normally when some form of energy is allowed to distribute itself in space, it tends towards a state of maximal uniformity. But in spontaneous focusing the reverse happens. The reasons for such focusing are important to understand. Conceptually, we seek a common understanding of why focusing arises in these different guises. Moreover, the concentrated energy seen in the examples above offers the potential for both benefit and harm. Deeper understanding can aid in controlling both the benefit and the harm.

The focusing seen in a crumpled sheet offers neither great benefit nor great harm. However crumpling provides a particularly clean and simple form of focusing. As shown below, crumpling occurs in any elastic manifold with a small spatial extent in one or more direction. Thus by studying crumpling, one may hope to shed light on a larger class of focusing phenomena. In the last decade there has been an upsurge of interest and activity in these focusing

phenomena. The purpose of this paper is to review the remarkable fruits of this activity. The paper grew out of a lecture series given at the Ecole de Physique et Chimie in Paris in 1999 and a summer school given at Altenberg, Germany in 2002 (Wood , 2002).

A. history

Crumpled structure has fascinated people for many centuries. Painters and sculptors have long been attentive to the ridges and gables in the flowing garments of their figures. First steps to a quantitative understanding came in Euler's analysis of incipient buckling in the 18th century (Euler , 1736). In this analysis, an initially unperturbed shape is subjected to an infinitessimal buckling deformation. Under sufficient external load one finds a mode of deformation that grows spontaneously in amplitude. This instability analysis gives information about initial stages of the crumpled structure, but it does not describe focusing. Soon afterward the geometric connections between compound curvature and strain were developed with great generality by Gauss (Millman, Parker, 1977). The formal basis for understanding strongly-deformed membanes came at the turn of the twentieth century with the Föppl–von Karman equations (Foppl , 1907; von Karman , 1956). Here the many constraints of mechanical equilibrium and differential geometry were exploited to reduce the many degrees of freedom of a sheet to just two scalar fields: a potential for the curvature tensor and a potential for the stress tensor. The two Föppl–von Karman equations in principle determine these two fields under appropriate boundary conditions. The two equations are of fourth order in derivatives and are in addition quadratic in the fields. In the years since World War II, several insightful approaches extended the power of the Föppl–von Karman equations beyond the realm of infinitessimal buckling, and into the regime known as postbuckling. Alexei Pogorelev (Pogorelov , 1988), Koiter, and Hutchinson, (Thompson *et al.* , 1984) enabled the prediction of the discontinuous buckling events that lead to crumpled structure. The nonlinear coupling in the Föppl–von Karman equations often leads to buckling events that are localized in the sheet. Such localized buckling amounts to the gathering of energy from the entire surface into a small region. This is a form of stress focusing that is an important precursor to the sharply focused structures treated in this paper. This subject was developed extensively in the 1980s and 1990s using concepts such as homoclinic orbits taken from dynamical systems theory (Lord *et al.* , 1997).

In the 1980's the connections between curvature and strain were shown to be important in controlling the shapes of thermally fluctuating membranes (Nelson *et al.* , 1989). The thermal fluctuations were shown to increase the rigidity of the membrane, with effective bending and stretching elasticity constants that varied anomalously with length scale (Guitter *et al.* , 1989). In this same period the numerical simulation of buckled membranes such as thin cylinders (Kergosien *et al.* , 1994) advanced greatly and accurately captured the focusing phenomena and bends seen experimentally.

In the 1990s several groups became interested in the scaling aspects of crumpled structure(Albuquerque, Gomes , 2002). In the early nineties using simplified deformations, the Chicago group demonstrated that the interaction between curvature and strain led to a scaling law for the focusing of energy (Lobkovsky *et al.* , 1995; Witten, Li , 1993). The scaling law applies to the asymptotic limit of thin sheets. It shows that the energy is concentrated principally in lines joining adjacent vertex points of maximal curvature. The energy is increasingly concentrated along these ridge lines as the thickness decreases. It is predominately contained in a fraction of the sheet that decreases in proportion to the 1/3 power of the thickness. The evidence for this scaling came from numerical simulations and non-rigorous energy balance arguments. Lobkovsky (1996a) was able to analyze one simplified geometry using the Föppl–von Karman equations. Applying standard methods of asymptotic analysis, he confirmed the 1/3-power scaling law noted above and deduced a number of other scaling properties, together with reduced equations for the ridge shape. Subsequently the Chicago group explored a variety of properties arising from the ridge singularities (Lobkovsky and Witten , 1997), including an experimental study of the strength of crumpled material that was consistent with the anticipated scaling law based on ridge energy (Matan *et al.* , 2002). In tandem with this work, a group at the Ecole Normale Superieure in Paris was studying more fundamental singularities: the individual vertices (BenAmar, Pomeau , 1997). They concentrated on a simplified geometry that they named the developable cone or d-cone. This is the shape obtained by pushing a piece of paper into a supporting ring using a point force (Figure 2). When a flat sheet is confined to a small volume such d-cones must appear. These are the vertices that terminate the ridges discussed above. Inspired by the Ecole Normale work, the group of L. Mahadevan in Boston was able to draw powerful conclusions about the shapes of d-cones using the fact that asymptotically these sheets become inextensible, with vanishingly weak strain (Cerda, Mahadevan , 1998). They showed how the stored energy grows with increasing deformation, and they showed several striking robust features of the shape. They explored the interaction of d-cones (Cerda *et al.* , 1999). Later the Ecole Normale group showed that d-cones move on a surface in response to distantly applied forces (Boudaoud *et al.* , 2000; Hamm *et al.* , 2004; Mora, Boudaoud , 2002). This group, and their collaborators in Chile and Boston simultaneously deduced striking scaling information about how the wavelength of *incipient* buckling

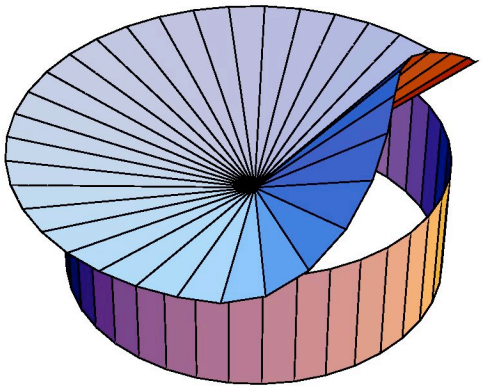

FIG. 2 Sketch of d-cone after Cerda, Mahadevan (1998); *cf* (Venkataramani *et al.* , 2000) Uncurved director lines are indicated.

depends on thickness in the presence of strain (Audoly , 1999; BenAmar, Pomeau , 1998; Cerda, Mahadevan , 2003; Cerda *et al.* , 2002). These wrinkling phenomena proved applicable to a great range of structures flowing from the nonlinear interaction between bending and strain (Belgacem *et al.* , 2002, 2000; Conti *et al.* , 2005; Sharon *et al.* , 2002). These wrinkling effects are distinct from focusing, since they don't describe the concentration of energy into an indefinitely small subset of the sheet. Thus we will not discuss them further in this paper.

B. interface focusing

The crumpling phenomena that we shall discuss belong to a rich and growing class of interfacial deformation phenomena. It seems worthwhile to review these phenomena to set the crumpling in context. We may classify these phenomena according to the constitutive nature of the interface being deformed, its dimensionality and the nature of the forces causing the deformation. The elastic membranes we described above are constitutively distinct from liquid membranes such as lipid bilayers (Safran , 1994) . Liquid membranes are characterized by a bending stiffness, but no shear modulus. They thus do not support static anisotropic shear stress within the membrane. There is no preferred distance between two given points. Thus the basis for focused crumpling is absent for such membranes. The rich variety of self-generated shapes in these membranes is thus quite different from the ones we will discuss. Liquid membranes can show *transient* phenomena akin to elastic membranes, since they develop viscous shear stress in response to flow (Boudaoud, Chaieb , 2001; da Silveira *et al.* , 2000; Debregeas *et al.* , 1998). While the membrane carries no cost for changing the distance between two points statically, it does carry a cost for changing this distance rapidly.

The surface being deformed may be either a free-standing membrane or the surface of a bulk liquid or solid. Surfaces of bulk matter show a range of distinct focusing phenomena of their own. Fluids may be splashed onto a surface (Xu *et al.* , 2005), or drawn into fine threads using viscous (Cohen, Nagel , 2002) or electrical (Ganan-Calvo , 1998; Shin *et al.* , 2001) forces. Inhomogeneous gels can show rich buckling patterns at their surface owing to differential deswelling (Chaieb, Melo , 1997; Matsuo , 1992) or delamination (Ortiz, Gioia , 1994; Tanizawa, Miura , 1978). Similar buckling occurs in the forced deformation of the Earth's crust owing to viscous stresses from the underlying mantle (Turcotte, Schubert , 2001). These patterns often show apparent sharp concentration of stress.

Liquid crystals show some aspects of elasticity and they show some stress-focusing phenomena that are closely analogous to those of elastic sheets. A smectic liquid crystal is a stack of fluid membranes held at a fixed separation. If one of these membranes is curved, the membranes within must curve more and more tightly, extrapolating to a focal point or line (Fournier, Virga , 1996).

Even the elastic membranes discussed below show a range of different deformation behavior according to the nature of the deforming forces and boundary conditions. One inevitable kind of forcing comes from equilibrium thermal fluctuations arising from exchange of thermal energy with the environment. As noted above, these thermal fluctuations give a flat sheet a much increased thickness, and this thickness imparts an induced bending stiffness to the sheet. Thermal fluctuations do not cause collapse or crumpling. By contrast, the forces imposed by a shrinking container may be expressed as normal forces applied on the points of the membrane depending on its position in space. As noted above, such forces when sufficiently strong do induce buckling and ultimately lead to crumpling. The structures seen in crumpling can also be induced by applying constraints as well as by applying forces. For example, the focusing seen in a d-cone is closely related to the conical structure produced by fastening two adjacent corners of

a rectangular sheet together and then fastening the two adjacent edges together. Likewise, the ridge structures seen in crumpling can be made by creating two such cones in a sheet, as explained below.

One major influence on the nature of crumpling is the dimensionality of the deformed object. We have noted that one-dimensional objects do not crumple while two-dimensional objects do. As for higher-dimensional surfaces, one may explore their response in the computer, as discussed below. An object in high dimensions has many ways to bend, twist and stretch. It is natural to expect new forms of stress focusing there. Understanding these can deepen our understanding of conventional crumpling. Moreover it enlarges our knowledge of how focusing can occur. Though we lack physical realizations of these high-dimensional objects, many physical phenomena are naturally described in spaces of different dimensions, such as the spaces used in string theory (Polchinski , 1998). Thus it is worthwhile to find the types of focusing that may occur.

C. prospectus

The following sections survey the recent findings about the nature of stress focusing in thin elastic sheets. Our emphasis is on the aspects that distinguish thin sheets from generic elastic bodies. Accordingly, we shall deal with the limiting behavior as the thickness becomes arbitrarily small relative to other characteristic lengths of the sheet. We begin our discussion in the next section by defining an elastic membrane and identifying its deformation energy. We shall note that thin confined membranes should approach the ideal of isometry: deformations must preserve the in-surface distance between adjacent points. With this motivation we discuss the classical consequences of isometric deformation: at every point at least one of the two principal curvatures must vanish. We recall how this local condition leads to global constraints: through each point passes a straight "director" line which must remain unbent to the boundary of the surface. We next see how the existence of two conical regions with converging directors conspires to create flat regions and a singular ridge line between the cone vertices. We then review how these properties generalize to manifolds with more than two dimensions embedded isometrically in spaces with more than three. When the embedding dimension is not too large, analogs of the unbent lines must appear. In a subset of these cases analogs of the ridge line appear as well. The existence of these unbent lines and their analogs prevents confinement of an isometric manifold into a region of limited linear size, such as a shrinking sphere. If such confinement is to occur, the constraint of isometry must be broken somewhere in the sheet. That is, the sheet must stretch somewhere. Simple arguments allow us to deduce the dimensionality of the required stretched regions.

In Section III we consider the simplest form of focusing seen in these sheets: the d-cone. We review the rich body of information derivable by considering the isometric limit. Simple equations yield the shape of the buckled surface and dictate certain invariants. A small idealization leads to a formulation in terms of Euler's Elastica (Euler , 1736). We discuss the core singularity and how its size should scale with thickness. We then compare these predictions with experimental and numerical observations. These observations confirm the properties that are independent of stretching but disagree with the predicted core thickness. We offer possible reasons for this disagreement. Next we consider the effect of the constraining rim of the d-cone on the nearby membrane. We recall recent numerical evidence of a striking geometric consequence. The mean curvature virtually vanishes at the contact line. We discuss the range of situations in which this vanishing is observed to occur.

In Section IV we deal with the ridge singularity induced by two d-cones or vertices. After showing a variety of ridge-producing configurations, we repeat several variational arguments that account for the degree of concentration of energy. We consider the implications of ridge focusing for a crumpled sheet with many ridges. We discuss how the energy of a ridge should depend on its bending angle. We then describe a variant of the ridge that shows different scaling and compare these two forms of ridge scaling.

In Section V we consider the differential equations of static equilibrium that dictate the state of stretching and bending of such membranes. These are the Föppl–von Karman equations mentioned above. We sketch the physical ideas leading to these equations and indicate how stretching effects regularize the singularities of the isometric limit. We recall the geometry known as the minimal ridge and recount Lobkovsky's asymptotic analysis of this ridge via the Föppl–von Karman equations. We discuss the scaling properties that emerge, emphasizing some striking nonlocal aspects of the crossover from the immediate vicinity of a vertex to the ridge region beyond.

In Section VI we review experimental data on individual ridges. These experiments—mostly numerical—have supported many of the scaling predictions of the previous section and have revealed unanticipated behavior. They also give a concrete guide to when the asymptotic predictions begin to describe materials of nonzero thickenss. We discuss exploration of ridge formation in more than three-dimensional space. To this end, we introduce a characterization tool for inhomogeneous energy focusing: the density of energy profile. Using this tool we show that ridge-like focusing occurs in higher-dimensional manifolds. We discuss numerical evidence supporting the predicted scaling properties of a ridge, including anomalous strength.

In Section VII we review the current knowledge about the collective properties of the multiple singularities produced

by crumpling. In simple geometries, experiments in Paris and Chile show how external stresses induce migration of d-cones. We then explore the implications of these scaling laws for the strength of real crumpled materials and review an experiment testing these implications. We discuss recent work about the statistical properties of the crumpled ridge network . We conclude by summarizing the many unanswered questions in crumpling and the strong incentives to answer them.

II. BASIC ENERGIES AND ISOMETRY

In this section we recall the standard mathematical description of a thin sheet of material embedded in space. We shall concentrate on sheets whose local deformation is arbitrarily weak, so that its internal forces are described by "linear elasticity." We shall contrast this weakly strained regime with other regimes in the course of the paper. To clarify the distinctions between these regimes we summarize their properties in Table I at the end of this section.

A. elastic energies

We first describe the elasticity of the material composing the sheet (Landau, Lifshitz , 1986). Each set $\underline{x} \equiv (x_1, x_2, x_3...)$ identifies a particular bit of matter. Physical materials have three material co-ordinates; we will generalize to higher dimensions in later sections. This material is embedded in space: to each point $(x_1, x_2, x_3, ...)$ we identify a point $\vec{r} \equiv r_1, r_2, r_3$ ... in space where the corresponding bit of matter is positioned. If the material is a solid, there is an energy functional $E[\vec{r}]$ that gives the elastic energy of the particular embedding $\vec{r}(\underline{x})$. This energy has a minimum for some particular $\vec{r}^0(\underline{x})$ and its rigid-body translations and rotations. One minimal $\vec{r}^0$ is given by $r_{01} = x_1, r_{02} = x_2; r_{03} = x_3, ...$ We set this minimal energy to zero. For a wide range of deformations, interactions between material points are local, and $E[\vec{r}]$ is a local functional in material co-ordinates. It depends only on the distances between nearby pairs of points; thus it can be expressed as a function of spatial derivatives such as $\partial r_3/\partial x_2 \equiv \partial_2 r_3$ or $\partial^2 r_1/\partial x_1 \partial x_2 \equiv \partial_1 \partial_2 r_1$. In the resting state of the solid, the distance ds between nearby points is given by $ds^2 = \sum_i {dx_i}^2$. However, embedding the membrane in space can alter this distance, so that ds^2 takes the form $g_{ij} dx_i dx_j$, where

$$g_{ij} = \frac{d\vec{r}}{dx_i} \cdot \frac{d\vec{r}}{dx_j} \equiv \delta_{ij} + 2\gamma_{ij}. \tag{1}$$

Evidently the (dimensionless) *strain tensor* $\boldsymbol{\gamma}$ may be taken as symmetric, and evidently in the undistorted state the strain tensor $\gamma_{ij} = 0$. Any small departure of γ_{ij} from 0 carries an energetic cost quadratic in γ. There are two independent isotropic scalars that are quadratic in a symmetric tensor; they may be taken as $(\mathrm{Tr}\,\boldsymbol{\gamma})^2$, and $\mathrm{Tr}\,(\boldsymbol{\gamma}^2)$. When we combine the requirements of translation invariance, positivity and the minimal state, we thus arrive at the form

$$E[\vec{r}] = \int_x \frac{1}{2}\lambda(\mathrm{Tr}\,\boldsymbol{\gamma})^2 + \mu \mathrm{Tr}\,\boldsymbol{\gamma}^2. \tag{2}$$

The Lamé coefficients λ and μ are properties of the material.

When the material is distorted uniformly so that some of the γ_{ij} are nonzero the work per unit strain $\partial E/\partial \gamma_{ij}$ is the force per unit area required to maintain the distorted state. This derivative is called the stress and is denoted σ_{ij}. Since the energy is quadratic in $\boldsymbol{\gamma}$, each component σ_{ij} is proportional to the various compnents of $\boldsymbol{\gamma}$. A commonly occurring case is when the solid is pulled in one direction (*eg.* direction 1) without other stress. Then the proportionality of that stress to the corresponding strain is called the Young's modulus Y. In terms of the Lamé coefficients, $Y \equiv \sigma_{11}/\gamma_{11} = \mu(3\lambda + 2\mu)/(\lambda + \mu)$. The solid then contracts in the orthogonal directions, *eg.* the 2 direction, by a factor $\gamma_{22} = -\nu\ \gamma_{11}$. The Poisson ratio ν is then given by $\nu = \frac{1}{2}\lambda/(\lambda + \mu)$. In what follows we shall consider *weakly strained* solids (*cf.* Table I), for which the strain γ is indefinitely small compared to unity everywhere. In this regime we are free to express energies, strains, curvatures etc. to lowest order in the strain. Remarkably, the strong focusing phenomena to be treated below are compatible with this weak-strain regime.

If the material has a very small extent in one or more dimensions, this description may be reduced. We consider a planar section spanned by material co-ordinates x_1, x_2, and having thickness h in the remaining direction. Then we may distinguish displacements $\vec{r} \cdot n$ normal to the sheet and those within the sheet. In the weakly-strained regime, the curvature tensor(do Carmo , 1976) C_{ij} may be defined by $C_{ij} \equiv \vec{n} \cdot \partial^2 \vec{r}/(\partial x_i \partial x_j)$. This is a symmetric tensor with dimensions of inverse length. In the absence of curvature, the stretching energy can be expressed in terms of the transverse or in-surface components 1 and 2 of the strain tensor.

For ordinary two-dimensional surfaces the energy of such a sheet may be expressed (Landau, Lifshitz , 1986) in terms of the in-surface strain tensor and the curvature tensor. To lowest order in these tensors the energy takes the form:

$$\begin{aligned} E[\vec{r}] &= S[\boldsymbol{\gamma}] + B[\mathtt{C}] \\ &= \int dx_1 dx_2 \left[\frac{1}{2}\hat{\lambda}\ (\mathrm{Tr}\,\boldsymbol{\gamma})^2 + \hat{\mu}\ \mathrm{Tr}\,(\boldsymbol{\gamma})^2\right] \\ &\quad + \int dx_1 dx_2 \left[\frac{1}{2}\kappa\ (\mathrm{Tr}\,\mathtt{C})^2 + \frac{1}{2}\kappa_G\left((\mathrm{Tr}\,\mathtt{C})^2 - \mathrm{Tr}\,(\mathtt{C})^2\right)\right]. \end{aligned} \tag{3}$$

The energy is the sum of a part S involving only the in-surface strain and another part B involving only the curvature. There are no cross-terms linear in $\mathtt{C}$ and $\boldsymbol{\gamma}$. Such terms would imply an asymmetry between one side of the surface and the other, which we shall suppose is absent. It is natural to denote S as the stretching energy and B as the bending energy. Again the derivatives of these energies give the local forces on a small element of surface. Specifically, $\partial S/\partial\gamma_{ij} \equiv \Sigma_{ij}$ is the membrane stress or force per unit length in direction j in the surface acting across a line in direction i. Likewise, $\partial B/\partial C_{ij} \equiv M_{ij}$, the torque per unit length in the j direction acting across a line in the i direction. A given set of stresses and torques acting on an element of surface also implies certain normal stresses denoted Q_i acting across a line in the i direction (Landau, Lifshitz , 1986; Mansfield , 1964).

The two-dimensional Young's modulus $\hat{Y}(= hY)$ relating uniaxial membrane stress to strain is related to $\hat{\lambda}$ and $\hat{\mu}$ by: $\hat{Y} = 4\hat{\mu}\ (\hat{\lambda}+\hat{\mu})/(\hat{\lambda}+2\hat{\mu})$. The membrane's Poisson ratio $\hat{\nu}(=\nu) = -\hat{\lambda}/(\hat{\lambda}+2\hat{\mu})$. The ratio of bending coefficients κ and κ_G to stretching coefficients λ and μ gives the relative importance of bending to stretching energy for a given deformation $\vec{r}(\underline{\mathrm{x}})$. The bending coefficients have dimensions of energy while the stretching coefficients have dimension of energy per unit length squared. Thus their ratios define characteristic lengths of the membrane. The length $\sqrt{\kappa/\hat{Y}}$ appears often in what follows. We call this length the *elastic thickness* and denote it by h_e. Many geometric properties of stress focusing depend on material properties only through h_e.

When the membrane is made of isotropic elastic material, the membrane constants $\hat{\lambda}$, $\hat{\mu}$ κ and κ_G are proportional to the material parameters λ and μ. We may also express $\hat{Y}$ and $\hat{\nu}$ in terms of λ and μ or the bulk Y and ν. Denoting μ/λ as m, the proportionalities are as follows:

$$\hat{\lambda} = \quad h\ \mu\ \frac{2}{1+2m} \quad = \frac{h\ Y\ \nu}{1-\nu^2} \tag{4}$$

$$\hat{\mu} = \quad h\ \mu \quad = \frac{hY}{2(\nu+1)} \tag{5}$$

$$\kappa = \ h^3\ \mu\ \frac{1+m^2}{3(1+2m)} \ = \frac{h^3\ Y}{12(1-\nu^2)} \tag{6}$$

$$\hat{Y} = \quad h\ \mu\ \frac{(3+2m)}{1+m} \quad = h\ Y \tag{7}$$

$$\hat{\nu} = \quad \frac{1}{2(1+m)} \quad = \nu \tag{8}$$

We note also that $h_e = h\ (12(1-\nu^2))^{-1/2}$. For ordinary materials where $1/3 < \nu < 1/2$, h_e varies from about $0.3h$ to $0.33h$.

Several aspects of the curvature bear pointing out. In order for the curvature field to represent a surface with a well-defined displacement field $\vec{r}(x)$, the curvature tensor must be "curl free" (do Carmo , 1976):

$$\partial_i C_{jk} = \partial_k C_{ji} \tag{9}$$

We note that κ_G is taken as the coefficient of the *difference* $\frac{1}{2}((\mathrm{Tr}\,\mathtt{C})^2 - \mathrm{Tr}\,\mathtt{C}^2)$. For the weakly strained surfaces considered here, this difference is the Gaussian curvature c_g (do Carmo , 1976); it is the product of the two principal curvatures, or eigenvalues of $\mathtt{C}$. The Gaussian curvature plays a special role in the sequel. The associated κ_G energy is strongly constrained by the *Gauss-Bonnet theorem* (Millman, Parker, 1977). The theorem is a purely geometric property of any smooth surface. It says that the integral of c_G over any surface is unchanged by smooth deformations of the surface that do not involve the boundary or its neighborhood. For weakly-strained surfaces whose energy is described by Eq. 3, the κ_G energy is unaffected by distortion of the surfaces.

Though the Gaussian curvature energy has no direct impact on the membrane configuration, it has a large indirect impact. This is because the presence of Gaussian curvature necessarily produces a strain field $\boldsymbol{\gamma}$: the curvature and

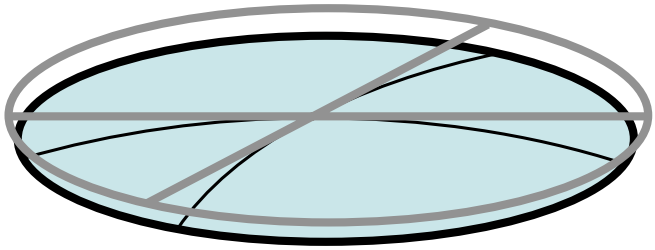

FIG. 3 Illustration of how Gaussian curvature leads to strain. A disk of radius ϵ on a flat sheet is shown by gray lines. The sheet is then curved downward with radial lines held fixed in length. The resulting spherical cap has a reduced perimeter shown as a heavy black line, indicating a compressive strain in the azimuthal direction.

strain fields are not independent. To illustrate this dependence, we denote the principal curvatures in the 1 and 2 directions as c_1 and c_2. Then with an appropriate choice of spatial co-ordinates $\vec{r}$, we may write

$$\vec{r} \cdot n = \frac{1}{2} c_1 {x_1}^2 + \frac{1}{2} c_2 {x_2}^2. \tag{10}$$

If $c_1 = c_2 \equiv c$, this region has the form of a spherical cap as shown in Figure 3. We suppose that the radial lines along x_1 and x_2 do not change their length under this deformation. However, a circle originally of radius ϵ becomes contracted by fraction $(\epsilon c)^2$. Evidently when c_1 and c_2 are both nonzero, the curvature is a source for strain. A uniform Gaussian curvature leads to a strain that grows quadratically with the size of the region. The general statement of this connection is Gauss's fundamental theorem of surfaces or Theorema Egregium (Millman, Parker, 1977)(do Carmo , 1976):

$$c_1 c_2 = 2\partial_1 \partial_2 \gamma_{12} - \partial_1 \partial_1 \gamma_{22} - \partial_2 \partial_2 \gamma_{11} + \mathcal{O}(\gamma^2) \tag{11}$$

The scaling of the above energies with thickness has strong implications about the relative importance of bending and stretching. The ratio of bending to stretching energy for any membrane configuration $\vec{r}(\underline{x})$ is proportional to $\kappa/\hat{\lambda}$ and $\kappa/\hat{\mu}$. Both of these ratios are proportional to the square of the thickness h. Thus thin membranes have a high energy cost to stretch relative to their cost of bending. That is, a very thin membrane responds to external forces almost like an unstretchable sheet. This observation motivates us to examine the behavior of membranes in the unstretchable limit, in which the in-surface strains are constrained to remain zero. Such membranes are called inextensible or "isometric."

B. isometric distortions

By definition an unstretchable distortion $\vec{r}(\underline{x})$ must have $\boldsymbol{\gamma} = 0$. Thus only the curvature $\mathtt{C}$ contributes to the energy. However, $\mathtt{C}$ is also constrained by the requirement of unstretchability, since as noted above Gaussian curvature produces strain. To avoid strain, we must require that the Gaussian curvature vanish everywhere. Thus at least one of the two principal curvatures must be zero at every point. If one follows the uncurved direction along the surface, the resulting line is straight in space (Eisenhart , 1909).

The impossibility of bending in all directions without stretching lies at the heart of the anomalous rigidity of *thermally fluctuating* membranes. Isotropic bending necessarily produces energetically costly stretching. Thus the bending is inhibited. The inhibition couples bending and stretching fluctuations. As we have seen, the amount of inhibition depends on the length scale of the fluctuation relative to the thickness. Achieving a mutual consistency between bending and stretching fluctuations results in a macroscopic bending stiffness and stretching moduli that depend on length scale via subtle power laws (Bowick, Travesset , 2001). These membranes may alternatively avoid the stretching cost by another dramatic accommodation. They may become macroscopically straight in one direction (Radzihovsky, Toner , 1998). In either of these scenarios, the system retains its unperturbed size in at least one direction. Thermal fluctuations do not lead to collapsed states like those imposed by a confining sphere.

The necessity of a straight line passing through every point imposes severe restraints on confining an isometric membrane. For example, if one wishes to bend the disk-shaped membrane in order to fit inside a sphere, the diameter of the sphere may be no smaller than that of the disk. One may allow somewhat greater confinement by allowing stretching near an isolated point. Then Gaussian curvature may occur near this "vertex." This allows a distortion in which the uncurved directions converge to the exceptional point, forming a cone-like structure.

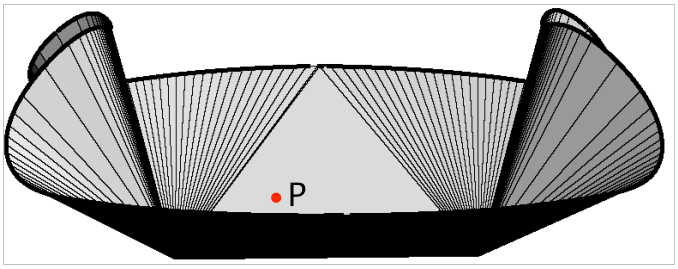

FIG. 4 A sheet with two d-cone vertices, after Cerda.nature.1999. The sheet is constrained to lie within a circular ring. The shape is calculated numerically using methods described in Section III.B. A generic point P near the line joining the vertices is marked. Unbent director lines are indicated.

The cone structure permits confinement in a sphere smaller than the disk diameter. However, as we reduce the sphere diameter to the radius of the disk, further reduction becomes impossible. To shrink the sphere further requires a second vertex. Evidently, the number of vertices required must increase continually if the membrane is to accommodate increasing confinement.

The presence of two vertices introduces a new effect on the surrounding surface. We see this by considering a generic point P in the vicinity of the two vertices, as shown in Figure 4. Isometricity requires that the line from the P to the first vertex be straight and unbent. The same is true for the line from P to the second vertex. Thus there must be two uncurved directions at P. Unless P lies directly between the two vertices, this condition forces both principal curvatures to be 0: there can be no curvature at P whatever.

Our requirement of no stretching thus has important consequences for the sheet, even beyond the vertices. The sheet is forced to have extended flat regions separated by sharp creases and thus infinite bending energy relative to the bending modulus κ. Here our assumption of unstretchability has clearly led to an unphysical conclusion.

To avoid this unphysical conclusion, we must recognize that even a very thin sheet has a non-infinite cost for stretching. By stretching, the membrane may avoid the infinitely sharp bending and attain a finite total energy. It is thus stretching that sets the scale of the stress focusing in the membrane. How stretching influences focusing is our main concern in the sections to follow. We first look more deeply at how isometry inhibits confinement by considering how the effect generalizes to higher dimensions.

C. higher dimensions

In the foregoing we have seen how very thin membranes become relatively difficult to stretch. We have seen further that unstretchable or isometric membranes respond to confinement by making strong deformations confined to small regions. This is the stress-focusing phenomenon that is the subject of our study. The necessity for focusing is a feature of the geometry of manifolds embedded in space. In order to understand this focusing more deeply, we now explore the range of situations when membranes show this focusing. To this end, we consider manifolds of different dimensionalities, such as a three-dimensional spherical ball embedded in a four, five, or six dimensional space.

As with ordinary membranes an m-dimensional manifold has a material coordinate system $\underline{\mathrm{x}} \equiv (x_1, x_2, \ldots x_m)$. Each point $\underline{\mathrm{x}}$ occupies some point $\vec{r}(\underline{\mathrm{x}})$ in the embedding space. The space points $\vec{r}$ have d coordinates $r_1, \ldots r_d$ with $d > m$. The strain tensor $\boldsymbol{\gamma}$ is given by Eq. 1, as before.

To see how curvature leads to strain in this general situation, we start from the undistorted state where $r_1 = x_1, r_2 = x_2, \ldots r_m = x_m, r_{m+1} = 0, \ldots r_d = 0$. As before we denote this state by $\vec{r}^{\,0}(\underline{\mathrm{x}})$. The directions $_{m+1}, \ldots, d.$ are evidently perpendicular or normal to the manifold. We now add a curvature near the origin by allowing $\vec{r}$ to depend quadratically on $\underline{\mathrm{x}}$. Curvature implies that $\vec{r}$ moves out of the $1, 2, \ldots, m$ plane as $\underline{\mathrm{x}}$ moves away from the origin. Thus to make the 1 axis curve into the positive $_{m+1}$ direction, we make $r_{m+1} = \frac{1}{2} C {x_1}^2$. To avoid strain in the 11 direction we must also correct the 1 component for the curving surface: $r_1 = x_1 - \frac{1}{6} C^2 {x_1}^3$. In vector notation, $\vec{r} = \vec{r}^{\,0} + \frac{1}{2} C {x_1}^2 \, \widehat{_{m+1}} - \frac{1}{6} C^2 {x_1}^3 \, \widehat{1}$, where $\widehat{1}, \widehat{2}, \ldots$ denote unit vectors along the embedding space coordinates. For a general curvature , each of the $d - m$ normal directions would be an arbitrary quadratic function of $x_1, \ldots . x_m$.

We first consider the analog of the strain seen above Eq. 11 for two-dimensional membranes, or 2-sheets. We suppose that the 1 and 2 axes each curve equally into the $_{m+1}$ direction. Thus the 1–2 plane of the manifold lies in the space spanned by the 1, 2, and $_{m+1}$ axes. This part of the system is evidently a two-dimensional spherically-curved membrane in a three-dimensional space. As in the example above Eq. 11, the strains γ_{11}, γ_{12} or γ_{22} must be nonzero. The m-dimensional manifold is not strain-free. The same argument shows that whenever two manifold axes curve into the same normal direction, these axes form a two-dimensional membrane in that normal direction having Gaussian

curvature and thence strain.

We may calculate the strain γ_{ij} explicitly for the case where the 1 and 2 axes curve into the $_{m+1}$ direction. Recalling the definition of strain from Eq. 1

$$\gamma_{ij} = \frac{1}{2}\left(\partial_i\ \vec{r}\right)\cdot\left(\partial_j\ \vec{r}\right) - \delta_{ij}. \tag{12}$$

Then

$$\vec{r} = \ \vec{r}^{\,0} + \frac{1}{2}c_1{x_1}^2\ \widehat{_{m+1}} - \frac{1}{6}{c_1}^2{x_1}^3\ \ \widehat{1} + \frac{1}{2}c_2{x_2}^2\ \ \widehat{_{m+1}} - \frac{1}{6}{c_2}^2{x_2}^3\ \ \widehat{2} \tag{13}$$

We first consider γ_{11}. By construction, it has equal and opposite contributions from the 1 and the $_{m+1}$ directions. The γ_{22} vanishes similarly. The $\gamma_{12} = \frac{1}{2}(\partial_1\ \vec{r})\cdot(\partial_2\ \vec{r})$ has a contribution from the $_{m+1}$ direction of magnitude $c_1c_2x_1x_2$. However, it has no contribution from the 1 direction since $(\partial_2\ \vec{r}) = -\frac{1}{2}c_2x_2 2\ \widehat{2} + c_2x_2\ \widehat{_{m+1}}$ has no such component. Similarly, it has no contribution from the 2 direction. Evidently γ_{12} is nonzero.

We now consider a case where two manifold axes curve into *independent* normal directions. We repeat the above analysis with the 1 axis curving as before into the $_{m+1}$ direction but now with the 2 axis curving into the $_{m+2}$ direction. The γ_{11} and γ_{22} vanish as before. However, now the γ_{12} vanishes as well. The ∂_1 factor now has only 1 and $_{m+1}$ components, while the ∂_2 factor has only 2 and $_{m+2}$ components. The dot product of the two is thus zero. We conclude that when all the axes curve into independent normal directions, strain is not generated.

It is often not possible for all the axes to curve into independent normal directions. The physical case of a 2-sheet embedded in 3-space is a case-in-point. Here we may, for example, bend the 1 material axis into the third dimension. But then there is no independent normal direction for the 2-axis to bend into. In order to avoid strain, the 2-axis must remain straight. The necessity of such straight directions inhibits confinement, as we discussed above. The same result follows whenever there are fewer normal directions than manifold directions, *i.e.,*whenever $d - m < m$, or $2m > d$. (Venkataramani *et al.* , 2000) Indeed, every reduction in d by 1 forces an additional uncurved direction. The number of uncurved directions is evidently $2m - d$. On the other hand, if $2m \leq d$, there is no requirement of uncurved directions. We may readily exhibit a configuration $\vec{r}(\underline{x})$ of arbitrarily small spatial extent with vanishing strain (Kramer , 1997). The following $\vec{r}(\underline{x})$ embeds a cube of side $2L$ into a sphere of radius $R\ m^{1/2}$:

$$\begin{aligned} r_1 = R\sin x_1/L; \quad r_2 \ &= \ R\sin x_2/L; \quad \ldots; \quad r_m = R\sin x_m/L \\ r_{m+1} = R\cos x_1/L; \quad r_{m+2} \ &= \ R\cos x_2/L; \quad \ldots; \quad r_{2m} = R\cos x_m/L. \end{aligned} \tag{14}$$

Each material axis has been curled into a circle of radius R with as many turns as necessary to accommodate the width L. One may readily use Eq. 12 to verify that $\gamma_{ij} = 0$.

This discussion shows the necessity of uncurved directions. It is natural to suppose that these locally uncurved axes align to form straight lines spanning the membrane. With 2-sheets in three dimensions this alignment is a familar fact. Its truth in higher dimensions is less obvious. If one follows a straight line in the material beginning in an uncurved direction, does it remain uncurved, so that the distance between its ends is the same as in the resting state? We know that each point along this line has an uncurved direction. It remains to show that the uncurved direction runs along the line we have defined. One may show this for a 2-sheet in three dimensions by considering a line that is everywhere tangent to the local straight direction starting from a point A as shown in Figure 5. We extend this line to a point B such that the transverse curvature has not changed sign between A and B. By construction, the surface has no curvature along this line; thus it remains in the tangent plane at A. We denote this line by C. We suppose that it is not straight and find that this leads to a contradiction. If C is not straight, then the straight line AB in the material from A to B is distinct from C and it meets C at a nonzero angle. Either AB lies in the tangent plane at A or it does not. If it does, then there are two independent uncurved directions at A: one along C, the other along AB. This contradicts our assumption that the surface is maximally curved. If AB does not lie in the tangent plane, then it must curve away from that plane. We consider a point D along the line AB close to A. We draw a perpendicular to AB at D and extend it until it meets curve C. This perpendicular is curved where it intersects the curve C, since it is not in the uncurved direction. By continuity, it is also curved at D. Thus D has curvature along both the AB direction and along the perpendicular. Thus by the Theorema Egregium, there is strain, contradicting the assumption that the deformation was isometric.

In higher dimensions locally straight directions also extend to form straight lines across the material (Venkataramani *et al.* , 2000). As with a 2-sheet this depends on the membrane being curved in other directions. One may see this by considering the two-dimensional material slice through the sheet spanning the locally straight direction and one of the curved directions. As before we adopt space coordinates that align with the material co-ordinates in directions 1 to m. We label the locally straight direction 1 and the locally curved direction as 2. This 2 axis curves into some normal direction that we denote as $_{m+1}$. We now consider the projection of the 1–2 material plane of the sheet into

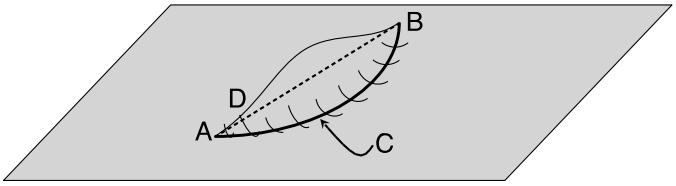

FIG. 5 Construction illustrating why locally uncurved directions remain uncurved to the boundary. The curve C is defined to follow the uncurved direction in the sheet. Its tangent plane is indicated by the shaded parallelogram. The line AB is a straight line in the material connecting the endpoints of C. Its path in space may depart from the tangent plane, as shown. The dashed line shows its projection on the plane. The curved surface near curve C is indicated by upward-curving lines perpendicular to C. The intersection of one of these lines with AB near A is marked D.

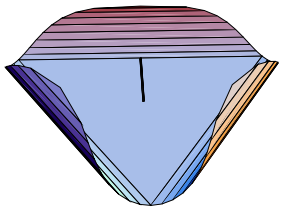

FIG. 6 If a sheet is not maximally curved, a straight line in the material that is uncurved in space at one point may become curved elsewhere. In the sheet pictured here the central region is flat and not maximally curved. The line drawn from the center is initially straight in space but then begins to curve, after Venkataramani *et al.* (2000).

the 1–2–$_{m+1}$ directions in space. This is evidently a 2-sheet embedded isometrically into a three-dimensional space. The theorem for ordinary sheets discussed above thus applies. It says that the 1 material axis cannot bend in the 2 or the $_{m+1}$ spatial directions. We now consider some other curved material axis, denoted 3. It cannot curve into the $_{m+1}$ direction. This would create strain, as discussed above. Thus it must curve into some orthogonal direction in the normal space. We call this the $_{m+2}$ axis. We now repeat the projection made above. This time we are projecting the 1–3 plane of the material into the 1–3–$_{m+2}$. space. Again applying the theorem for 2-sheets, we conclude that the 1 axis cannot bend into the 3 or $_{m+2}$ directions.

We may repeat this reasoning for all material directions with curvature. There are at most $d - m$ such directions. For such "maximally curved" sheets, our argument in the last paragraph shows that the 1 axis cannot curve into any normal direction. By construction it does not curve in any material direction. Thus it must be uncurved in all directions. It is a straight line in space, and it must remain straight to the boundary, as with 2 sheets in 3 space. We've thus shown that any point with maximal curvature has a straight line extending from that point to the boundary. This straight line prevents confinement within any sphere smaller than the length of the line. Thus for example if the m sheet is a ball of diameter L and if the center has maximal curvature, there must be a straight line of length L. It cannot be confined without stretching in a sphere of diameter smaller than L.

This argument has added power for higher-dimensional manifolds, such as a 3-sheet in 4 space. Here a maximally curved sheet can have only one curved direction. Two directions must be uncurved at every point. Labeling these directions 1 and 3, we infer that arbitrary points in the 1–3 plane of the material must remain flat in space. In general all the k locally flat directions extend to form a flat k-dimensional subspace in the embedding space.

We've argued that there can be no confinement without stretching in the most obvious case of maximal curvature, whenever $d < 2m$. A less obvious case occurs if the curvature is not maximal anywhere. An example is a two-dimensional disk that has no curvature at the center. Such as disk may nevertheless have curvature elsewhere, as in the three-cornered-hat configuration pictured in Figure 6. Lines extending in uncurved directions from the origin may begin to curve elsewhere. One may imagine the possibility that a sheet with $d < 2m$ might be confined by avoiding maximal curvature everywhere. To rule out such possibilities requires subtle mathematical reasoning (Venkataramani *et al.* , 2000), which we do not reproduce here. This reasoning proves that every point has a straight line extending essentially to the boundary. Moreover, this reasoning suggests that every point has a flat $2m - d$ subspace that extends to the boundary. Though this stronger suggestion has not been proved, we shall assume it in what follows.

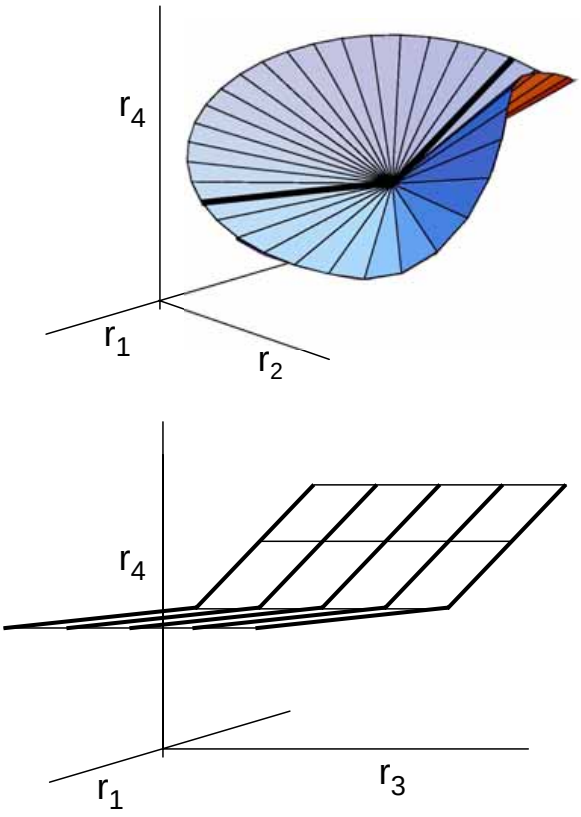

FIG. 7 Simple vertex line in a three-dimensional sheet made by stacking two-dimensional sheets, *cf.* DiDonna *et al.* (2002). Shown are two cross sections of the sheet. Material co-ordinates are x_1, x_2, x_3; space co-ordinates are r_1, r_2, r_3, r_4. Upper picture shows the image of an x_1–x_2 cross-section, embedded in the r_1–r_2–r_4 hyperplane of the space. All parallel cross sections cut perpendicular to the x_3 axis are identical to this one. The image of the x_1 material line is marked by a heavy line. Lower picture shows the image of the x_1–x_3 plane. Each heavy broken line is the image of an x_1 material line. The vertex line is the set of break points of these lines, extending along the x_3 direction.

1. stretching vertices

In the previous section we recalled that one may decrease the confinement radius by allowing stretching at isolated points or vertices. Thus one such vertex at the center of a disk of diameter L allows us to break the straight directors of length L in half, thus permitting cone-like structures of size $L/2$ as in Figure 2. By allowing stretching at the vertex, we have in effect modified our isometric sheet by creating a tiny hole at the vertex. The hole forms one boundary of the sheet, and straight director lines may terminate there. By allowing more vertices in the sheet, one may confine it to smaller spheres. If we place enough vertices in the sheet so that their separation is less than about b, all points of the sheet lie within a distance b of the (internal) boundary. Thus the director lines need be no longer than b, and confinement within a confining width b is possible.

For sheets of higher dimensionality one may also introduce vertices in order to permit confinement (DiDonna *et al.* , 2002). To illustrate this possibility, we form a 3-sheet in four dimensions by stacking many copies of a d-cone like that of Figure 2 into the fourth dimension to create a 3-sheet like Figure 7. This 3-sheet has no strain, and it is confinable in the first three directions to a distance $L/2$. In order to enable this much confinement, isolated point vertices were not sufficient. Instead, the vertex region has become a line. The internal boundary required is one-dimensional.

This example shows that vertices must be more than isolated points if they are to permit confinement of arbitrary manifolds. We argued above that m-sheets in d dimensions must have flat $2m - d$ subspaces that extend to the boundary. In order to confine such a subspace to diameter b all points of this subspace must be less than $b/2$ from the boundary—either the exterior boundary or an internal vertex boundary. The dimensionality of this boundary is that of the surface of the subspace in question, namely $2m - d - 1$. Our vertices must have a dimensionality at least as great in order to permit confinement (DiDonna *et al.* , 2002).

The dimensionality of these vertices increases progressively as we decrease the embedding dimension. To show this, we consider an m-dimensional ball of diameter L in a space of large dimension d. If $d = 2m$, then the ball is

confinable to arbitrarily small diameter without stretching. Each material axis may be curled into a circle into an independent normal direction, and this causes no strain. Now if we decrease the embedding dimension by 1, there must be uncurved lines extending to the boundary. In order to allow confinement to diameters $b \ll L$ requires many point vertices separated by distances of order b or less. In principle, pointlike vertices may not suffice, but empirical evidence given below indicates that isolated points are sufficient. If we again decrease d by one, then there are flat two-dimensional spaces in the manifold extending to the boundary. In order to confine this manifold, we require one-dimensional vertices. These must form a network so that all points lie within a distance of order b from a vertex. Empirically, as noted below in Section VI these vertices consist of straight-line segments. If we decrease d again, the flat regions become three-dimensional and the vertices become two-dimensional surfaces. Finally we reach the smallest possible d, namely $m+1$. At this point, the manifold must have $m-1$ flat directions. These form hyperplanes in the manifold. To allow confinement, we need a network of $(m-2)$-dimensional vertices.

2. ridges

In our description of confining a 2-sheet in Section II.B we encountered a new element of structure in addition to the vertices. We observed that typical points in the sheet were constrained by more than one nearby vertex. The line pointing towards each vertex was required to be straight. In general the lines are not colinear. This implied that a region of the sheet had two independent uncurved directions, and thus was entirely flat. The curvature was concentrated in a vanishing fraction of the material. The confinement process induced singularities called ridges in addition to the vertices. The conditions for this enforced flatness are not completely clear, even for ordinary sheets. Figure 4 (Cerda *et al.* , 1999) shows that two vertices do not suffice to flatten an entire sheet. Instead, only triangular regions whose tips are at vertices or elsewhere on the exterior boundary become flat.

Clearly ridge formation must occur for higher-dimensional sheets. This is readily apparent when $d = m + 1$. We suppose that our m-sheet has been strongly confined, so that there are vertex points at distance less than $b \ll L$. We note that there is only one allowed direction of curvature; thus the surface at a generic point P is either maximally curved or flat. We first suppose that it is maximally curved. Then there is a flat $m-1$-dimensional uncurved space surrounding it, extending to a vertex boundary. We identify the nearest vertex point V on this boundary. This point extends to an $m-2$ dimensional manifold. We consider the 2-surface in the material that includes the line PV and a second line through P normal to the vertex manifold. This 2-surface may be analyzed like an ordinary sheet in three dimensions.

Within our 2-surface, the original vertex point is an isolated point. However, there are in general other vertex points lying elsewhere in the 2-surface. We consider the closest one to P. The situation in this 2-surface is similar to that in an ordinary surface. We thus expect that flattened regions like those found in an ordinary surface must occur. These flattened regions should be bounded by straight lines joining pairs of vertex points. In general the flat regions meet at a nonzero dihedral angle, and thus the boundary line is sharply bent. This is the analog of the ridge in an ordinary sheet. Since the intersection of a ridge with a 2-surface is one-dimensional, the overall dimensionality of a ridge is expected to be one less than that of the manifold, that is, $m-1$.

Our understanding of ridges is sufficiently weak that we do not fully understand the conditions for their existence even for ordinary 2-sheets. Our understanding of m sheets in $m+1$ dimension is weaker, and for higher embedding dimensions, it is weaker still. However, empirical evidence gives a fairly clear-cut conclusion, as we discuss in Section VI below.

To conclude this section we list the properties of weakly strained elastic sheets in Table I. We compare these with unrestricted deformations and with isometric and weakly-deformed sheets.

In the next section we return to ordinary two-dimensional sheets and discuss the most basic form of focusing by considering the structure called the d-cone.

TABLE I Regimes of deformation of an elastic sheet of thickness h and width L confined in a sphere of radius R. The columns list various regimes that can occur in such a sheet of m dimensions in d dimensional space. The properties for ordinary 2-dimensional sheets in 3 dimensional space are indicated in the last row.

	non-weak strain	**weak strain**	**isometric**	**weak deformation**
definition	Strain in some regions is of order unity or larger.	All strain in material is small enough to be treated to lowest order.	Strain in material directions vanishes everywhere.	Displacement from a relaxed reference state is small enough to be treated in lowest order.
example	sheet confined in sphere with $R \simeq h$	thin sheet of paper	arbitrarily thin sheet of paper	vibrating drum head
description	no restrictions on amount of bending and stretching.	resembles isometric sheet, but singularities are replaced by small regions of high curvature does not require weak deformation	gently curved regions punctuated by singular boundaries of infinite curvature	Slope relative to reference state is small everywhere. no sharp curvature implies weak strain
relation to this paper	mentioned	central subject	treated	mentioned
configuration specified by	strain field in all d dimensions of the sheet	strain and curvature fields in m dimensions	curvature field in m dimensions	*eg.* local height above reference position
energy functional	depends on material	quadratic in strain and curvature, Linear elasticity is valid. Minimum-energy configuration satisfies Föppl–von Karman equations.	quadratic in curvature	quadratic in height and its gradients
thickness regime	unrestricted	$h \ll L$, $h \ll R$ $h \ll$ inverse curvature everywhere	$h = 0$	$h \ll$ inverse curvature
confinement to $R \ll L$	unrestricted	ok if h is sufficiently small	only if $d \geq 2m$ or if singularities are allowed †	no. incompatible with definition
types of focusing		*vertices:* if $d < 2m$††‡‡ dimension $2m - d - 1$ ††‡‡ *ridges:* if $d = m + 1$ ††‡‡ dimension $m - 1$ bending energy is 5 times stretching energy ‡‡ width $\sim h^{1/3}$ ‡‡	*vertices:* if $d < 2m$ † *ridges:* if $d = m + 1$ ††	none
sheets in 3 dimensions		point vertices joined by linear ridges	point vertices, linear ridges	

† proved analytically.

†† strongly indcated by analytical arguments.

‡ strongly suggested by energy-balance arguments.

‡‡ consistent with numerical experiments.

III. D-CONES

If one pushes an infinitely thin sheet into a circular opening, as in Figure 2, the surface deforms so as to avoid stretching almost everywhere. As discussed in the previous section, the deformation can create curvature in only one direction at any point. An unbent "director" line passes through each point. Such a surface is called developable. In Figure 2 the directors converge to a point to form the cone-like geometry called a developable cone or d-cone (Cerda, Mahadevan , 1998). The surface is developable except at the convergence point. The act of exerting a simple force

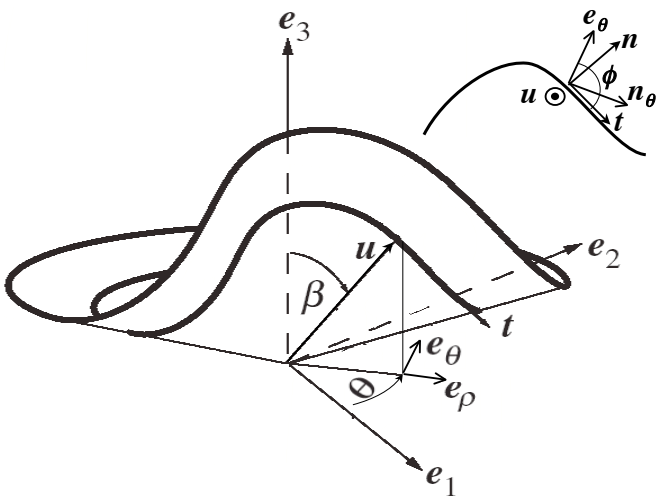

FIG. 8 Co-ordinates for analyzing the shape of the d-cone after Cerda, Mahadevan (2005a). The unit vector $\widehat{u}(s)$ points from the vertex to a point on the unit circle at a distance s from the center of the buckled region. The Cartesian basis vectors $\widehat{e}_1, \widehat{e}_2, \widehat{e}_3$ are shown. The polar angle β and azimuthal angle θ and the polar basis vectors $\widehat{e}_\rho, \widehat{e}_\theta, \widehat{e}_3$ are indicated. The inset shows the region near s viewed along the radial line $\widehat{u}$. The tangent unit vector $\widehat{t}$ is shown on the main picture and the inset. The normal unit vector $\widehat{n}$ is shown on the inset only. The inset defines the angle ϕ between $\widehat{t}$ and $\widehat{e}_\theta$, as well as the $\widehat{n}_\theta$ unit vector needed to form a basis with $\widehat{u}$ and $\widehat{e}_\theta$.

has thus organized the entire material. Moreover the structure is similar to the vertex structures that appear in a crumpled sheet, as discussed in the last section. The d-cone geometry captures the roof-gable shape seen at the intersection of folds in draped clothing. It is clearly of fundamental interest.

In this section we discuss the properties of d-cones. We begin by considering the unstretchable limit, in which the shape is strictly developable except at the vertex point. In a real material of finite thickness, this simple description is modified. The vertex point expands to a core region of finite size in which stretching is important. We discuss how bending and stretching energies determine the size and energy content of this core. Departures from the ideal developable shape also occur where the surface contacts the constraining ring. We discuss a striking regularity in the shape at this ring.

A. kinematics

The ideal d-cone is strongly constrained. Its shape is described by one scalar variable in one dimension. We may see this by drawing a circle of unit radius in the sheet concentric with the forcing point, following the discussion of Cerda, Mahadevan (2005a). The angular position of a point on this circle is denoted s. When the d-cone is formed, the director lines are radial lines. The only curvature occurs in the azimuthal direction. We denote this azimuthal curvature by $c(s)$. Determining this $c(s)$ thus determines the shape of the surface.

To describe the constraint imposed by the container, we now consider the position of this circle in space in the deformed sheet as shown in Figure 8. We place our coordinate origin at the vertex, so that the point at s has a position $\widehat{u}(s)$ where $\widehat{u}$ is a unit vector. Evidently $\widehat{u}(s)$ maps out a curve in space. We define a vertical, polar coordinate axis perpendicular to the plane of the constraining ring. We define the polar angle of $\widehat{u}(s)$ as $\beta(s)$ and denote the azimuthal angle by $\theta(s)$. The ring itself has a polar angle β_0. Since the surface must lie within the ring, $\beta(s)$ must be less than or equal to β_0 for all s.

In order to minimize the energy subject to this constraint, we must evidently relate $\beta(s)$ to $c(s)$. To this end we define the tangent unit vector $\widehat{t}(s)$ and note that $\widehat{t} = \dot{\widehat{u}}$, where the dot over the symbol denotes the derivative with s. Since $\widehat{t}$ is the derivative of a unit vector, $\widehat{t} \perp \widehat{u}$. Likewise, $\ddot{\widehat{u}} = \dot{\widehat{t}}$ is perpendicular to $\widehat{t}$ and its magnitude is the curvature of curve $\widehat{u}(s)$. We may form a normal unit vector to the sheet $\widehat{n}$ via $\widehat{n} \equiv \widehat{t} \times \widehat{u}$.

The curvature of $\widehat{u}(s)$ is distinct from the curvature of the surface. $\widehat{u}(s)$ has a curvature within the material as well as following the curvature of the sheet. The curvature $c(s) = -\widehat{n} \cdot \dot{\widehat{t}} = -\widehat{n} \cdot \ddot{\widehat{u}}$. The sign of $c(s)$ is chosen so that inward

curvature is positive. In order to relate $c(s)$ to β, it is useful to specify the motion of the $\widehat{u}(s)$ curve relative to the azimuthal direction $\widehat{e}_\theta$. We note that $\widehat{e}_\theta$ is perpendicular to $\widehat{u}$ and thus it is in the plane of $\widehat{n}$ and $\widehat{t}$. The direction normal to $\widehat{e}_\theta$ and $\widehat{u}$ is denoted $\widehat{n}_\theta$.

The complete curve may now be specified in terms of the angle ϕ between $\widehat{t}$ and $\widehat{e}_\theta$. To this end we note that $\widehat{t}$ in the $\widehat{e}_\theta$–$\widehat{n}_\theta$–$\widehat{u}$ basis takes the form

$$\widehat{t} = \cos\phi\ \widehat{e}_\theta + \sin\phi\ \widehat{n}_\theta. \tag{15}$$

The derivative $\partial\widehat{t}/\partial\phi$ amounts to a rotation of $\widehat{t}$ into the $\widehat{n}$ direction, *i.e.,* $\partial\widehat{t}/\partial\phi = -\widehat{n}$. To relate ϕ to the curvature, we compute $c(s) = -\widehat{n}\cdot\dot{\widehat{t}}$:

$$\widehat{n}\cdot\dot{\widehat{t}} = \widehat{n}\cdot\frac{\partial\widehat{t}}{\partial\phi}\dot{\phi} + \cos\phi\ \widehat{n}\cdot\dot{\widehat{e}}_\theta + \sin\phi\ \widehat{n}\cdot\dot{\widehat{n}}_\theta. \tag{16}$$

The first term is simply $-\dot{\phi}$ as noted above. To compute the other terms, we first express the vectors in our $\widehat{e}_\theta$–$\widehat{n}_\theta$–$\widehat{u}$ basis. First, we note that since $\widehat{n}\perp\widehat{t}\perp\widehat{u}$, $\widehat{n}$ must have the form $\sin\phi\ \widehat{e}_\theta - \cos\phi\ \widehat{n}_\theta$. We observe that $\dot{\widehat{e}}_\theta = -\dot{\theta}\widehat{e}_\rho$, where $\widehat{e}_\rho$ is perpendicular to $\widehat{e}_\theta$ and the polar axis: $\widehat{e}_\rho = -\cos\beta\ \widehat{n}_\theta + \sin\beta\ \widehat{u}$. Finally, $\dot{\widehat{n}}_\theta$ must lie in the $\widehat{e}_\theta$–$\widehat{u}$ plane. Specifically, $\dot{\widehat{n}}_\theta = -\dot{\theta}\cos\beta\ \widehat{e}_\theta + \dot{\beta}\ \widehat{u}$. Combining, we find:

$$\begin{aligned}
\widehat{n}\cdot\dot{\widehat{e}}_\theta &= (\sin\phi\ \widehat{e}_\theta - \cos\phi\ \widehat{n}_\theta)\cdot(-\cos\beta\ \widehat{n}_\theta + \sin\beta\ \widehat{u})(-\dot{\theta}) \\
&= (-\dot{\theta})(\cos\phi\ \cos\beta) \\
\widehat{n}\cdot\dot{\widehat{n}}_\theta &= (\sin\phi\ \widehat{e}_\theta - \cos\phi\ \widehat{n}_\theta)\cdot(-\dot{\theta}\cos\beta\ \widehat{e}_\theta + \dot{\beta}\ \widehat{u}) = (-\sin\phi\ \cos\beta\ \dot{\theta}).
\end{aligned} \tag{17}$$

Using these results we may now express $\widehat{n}\cdot\dot{\widehat{t}}$ as

$$\begin{aligned}
\widehat{n}\cdot\dot{\widehat{t}} &= -\dot{\phi} + \cos\phi(-\dot{\theta})(\cos\phi\ \cos\beta) + \sin\phi(-\sin\phi\ \cos\beta\ \dot{\theta}) \\
&= -\dot{\phi} - \cos^2\phi(\dot{\theta})(\cos\beta) - \sin^2\phi(\dot{\theta}\cos\beta) \\
&= -\dot{\phi} - (\dot{\theta})(\cos\beta).
\end{aligned} \tag{18}$$

Finally, $\dot{\theta}$ can readily be expressed in terms of ϕ, We see this by expressing $\dot{\widehat{u}} \equiv \dot{\widehat{t}}$ in the standard $\widehat{e}_\theta$–$\widehat{e}_\rho$–$\widehat{e}_3$ co-ordinates:

$$\dot{\widehat{t}} = \dot{\theta}\ \sin\beta\ \widehat{e}_\theta + \dot{\beta}\ (\cos\beta\ \widehat{e}_\rho - \sin\beta\ \widehat{e}_3). \tag{19}$$

The component along $\widehat{e}_\theta$ must be the same as in Eq. 15. Thus, $\sin\beta\ \dot{\theta} = \cos\phi$, so that

$$c(s) = -\widehat{n}\cdot\dot{\widehat{t}} = \dot{\phi} + (\cos\phi\ \cot\beta). \tag{20}$$

To close the equation, we note that the $\dot{\beta}$ component of $\dot{\widehat{t}}$ in Eq.19 is precisely the component perpendicular to $\widehat{e}_\theta$ in Eq. 15, so that $\dot{\beta} = -\sin\phi$.

For a given $\phi(s)$, we may now determine $\beta(s)$ and $\theta(s)$ and thence $c(s)$. Thus we may evaluate the energy for any d-cone surface. Conversely if $c(s)$ is given, we may find $\phi(s)$ by solving Eq. 20 viewed as a differential equation for ϕ. In the next section we show how mechanical considerations determine $c(s)$.

B. mechanics

To find the shape of the d-cone, we must minimize the bending energy B of Eq. 3. Specifically, the energy lying between a minimum radius R_* and a maximum radius R_p is given by

$$B = \frac{1}{2}\kappa\int_{R_*}^{R_p} r\ dr\int_0^{2\pi} ds\ (c(s)/r)^2 = \frac{1}{2}\kappa\log(R_p/R_*)\int_0^{2\pi} ds\ c(s)^2. \tag{21}$$

We first note the overall scaling of the energy with system size. Being proportional to the dimensionless material constant κ, this energy cannot vary as a power of the system size. Instead, a logarithmic growth with system size is dictated. The energy also diverges as the inner radius near the vertex goes to zero. The remaining dependence on curvature is simple. It remains to minimize this energy under the proper constraints in order to infer $c(s)$.

The formal constraint from the last subsection, $\beta < \beta_0$ bears on $c(s)$ only very indirectly. There is no obvious way to implement this constraint in the minimization. However, one may simpify this problem enormously by anticipating the qualitative shape of the surface (Cerda, Mahadevan , 2005a). The surface consists of a contacting region that follows the constraining ring and a buckled region that does not touch the ring. The constraint on the buckled region is simple. It has a constrained displacement between its ends. Thus the buckling takes the same form as the classic Euler buckling of a thin, compressed rod (Cerda, Mahadevan , 2005a; Mansfield , 1964). The equation for the shape of the buckled region is thus[1]

$$\ddot{c} + (a^2 + \frac{1}{2}c^2)c = 0. \tag{22}$$

The constant a arises from the constraint. We anticipate that the buckled region is symmetric about $s = 0$; thus $\dot{c}(0) = 0$. The buckled region extends to some $s = s_c$ called the "takeoff angle", as yet unknown. At takeoff, the curvature attains a value c_c. For given values of s_c, c_c and constraint constant a, the buckled profile $c(s)$ is uniquely determined. These three constants are determined by three matching requirements at s_c. a) The unbuckled region must have length $s = 2\pi - 2s_c$. b) The normal stress across the boundary Σ_{ss} must be equal in the buckled and unbuckled region. c) The torque or moment exerted at s_c by the two sides must be equal. Naturally, the magnitudes, *eg.* $c(s_c)$ depend on the angular depth $\pi/2 - \beta_0$ of the d-cone. The unbuckled region has a constant $c(s)$ and is under a constant compressive stress, independent of s. The constraining ring exerts a constant normal force P in order to impose the constraint.

In order to determine the shape of the surface, and the angular span s_c of the buckled region, it is necessary to find not merely the curvature profile $c(s)$, but also the director angle profile $\beta(s)$. For this, one must solve the additional kinematic equation 20 and determine $\phi(s)$. The solutions have been explored explicitly in the elegant work of Cerda, Mahadevan (2005a). We now discuss some noteworthy results.

take-off angle: The most fundamental geometric characteristic of the buckling is the take-off angle s_c. Remarkably the limiting value of $2s_c$ for small displacement is not zero but is about 2.43 radians or 139 degrees.

take-off force: In our specification of the problem, we required the normal stress and torque to be continuous at the takeoff point; however, we did not specify the curvature derivative $\dot{c}_c$. There is thus no reason for $\dot{c}_c$ to vanish as it does in the unbuckled region. Indeed, one finds that $\dot{c}_c$ is different from the unbuckled curvature derivative, so that the curvature derivative must change discontinuously at takeoff. As with a bent rod, this change requires a localized normal force called the take-off force to act at the takeoff point. One may readily see the mechanical necessity for this force by considering the force and torque equilibrium for the entire sheet assuming no take-off force. The vertical pushing force at the center must be balanced by the uniform ring forces acting over an angular distance $2\pi - 2s_c$. The ring forces must act normal to the sheet, so the direction of the resultant ring force is fixed. We may choose the pushing force to balance this resultant. However this choice does not provide a balance of torques. Some further external force is needed. This need is filled by the take-off force, and the torque-balance requirement gives a simple way to calculate its magnitude. Evidently, the total take-off force is of the same order as the central pushing force. In the weak-buckling limit, the take-off force is 0.411 of the pushing force (Cerda, Mahadevan , 2005a; Liang, Witten , 2005) . These concentrated forces at the self-selected take-off points represent a form of focusing.

Given the shape of the sheet, it is straightforward to calculate the forces acting on any part of the sheet (Cerda, Mahadevan , 2005a). Each element of the sheet is subject to stress and to bending moments. The bending moments are proportional to the curvature through the bending stiffness κ. Since all bending is in the transverse direction, all bending moments on an element act on its transverse sides. For the unbuckled part of the sheet, a normal pressure P from the container also acts. Here the principal axes of the stress are the radial and transverse directions. To

---

[1] This equation for the shape of a bent plate emerges naturally from the Föppl–von Karman equations to be presented in Section V.A. It may be derived simply from the more transparent Kirchhoff (Love , 1944) formulation for the bending of a line of local curvature $c(s)$ and energy $\frac{1}{2}B\int_0^t ds\ c(s)^2$ in a plane. The energy is to be minimized with one end fixed and with a given force F and bending moment M acting on the opposite end. In the Kirchhoff picture, one uses the angular orientation $\alpha(s)$ at s to specify the shape of the line. Evidently $c = \dot{\alpha}$. The applied force adds an energy $\int F\cos\alpha\ ds$. Thus the energy to be minimized is a functional of α and $\dot{\alpha}$. It has the form of Hamilton's principle of classical mechanics (Marion, Thornton , 1995). The angular variable α that minimizes the energy satisfies the Euler-Lagrange equation $B\ddot{\alpha} - F\sin\alpha = 0$. Such a classical motion conserves the value of the Hamiltonian $H \equiv \frac{1}{2}B\dot{\alpha}^2 - F\cos\alpha$: H is independent of s. Equation 22 may be shown equivalent to the Euler Lagrange equation by differentiating the latter once to obtain $B\ddot{c} - F\cos\alpha\ c = 0$. To eliminate α one observes that $F\cos\alpha = \frac{1}{2}B(\dot{\alpha})^2 - H = \frac{1}{2}Bc^2 - H$. Renaming H as $-B\ a^2$ the Euler-Lagrange equation has the form of Eq. 22. The force F may be viewed as a Lagrange multiplier imposing a constraint of fixed distance between the ends of the line in the F direction. The bending moment M does not enter the equations but merely influences the boundary curvature at the end of the line.

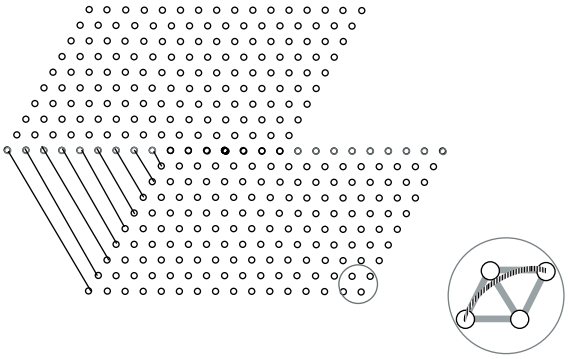

FIG. 9 Lattice of springs to simulate an elastic sheet, after Seung, Nelson (1988). Inset at right shows nearest neighbor springs (light lines) and spring between adjacent triangles to impart bending stiffness (dark line). One may make a disclination cone by removing a sector of the lattice and joining the boundary particles with springs as shown by the lines at lower left. If both sectors are joined in this way, the minimum-energy shape of the surface has the boat shape shown in Figure 11. Inset to Figure 10 shows a hexagonal section of a similar lattice deformed into a d-cone.

maintain the imposed curvature $c(s)$ in the contacting region, this P must be nonzero. To maintain the conical r dependence of the shape, this P must also have a prescribed r dependence; one finds that[2] $P(r) \sim r^{-3}$. That is, if one strictly enforces the conical shape, *eg.* by pushing the sheet into a conical container of opening angle β, the constraint force P is concentrated towards the center. It diverges at the center; the total force acting within a distance r also diverges. This contrasts with the experimental geometry of Figure 2, in which the constraining force is only applied at a circular boundary. The internal stresses in the two cases are also qualitatively different. In the ideal case, the balance of normal forces dictates a compressive stress Σ_{ss} in the azimuthal direction. Much of this stress is needed to balance the external pressure P from the conical container. However, in the absence of P, one readily verifies (Liang, Witten , 2006) that Σ_{ss} must become tensile. (One may verify it physically by noting that there is a positive Gaussian curvature creating a slight outward bulge in the surface. One may also create a small radial cut in a paper surface and note that the edges of the cut spread apart when the paper is deformed into a d-cone shape.) This example shows that caution is needed in interpreting the unstretchable limit, even in regions where the shape is arbitrarily close to the limiting unstretchable shape.

C. core region

Our central concern in examining the d-cone is to understand the degree of focusing of stress and energy. The constraint of near unstretchability clearly causes strong focusing at the vertex of the d-cone. This focusing even causes a logarithmic divergence in the total energy. The degree of focusing is evidently measured by the size R_* of the region where the approximation of unstretchability breaks down. That is, the radial curvature C_{rr} becomes comparable to the azimuthal curvature C_{ss}, or the Gaussian curvature becomes comparable to the square of the mean curvature. In the late nineties the work of BenAmar, Pomeau (1997) and Cerda, Mahadevan (1998) drew attention to the peculiar nature of this region. It contrasts with the vertex region of a simple cone made by fastening two edges of a sheet together as in Figure 9. In a simple cone the material also stretches near the vertex to avoid an infinite energy. The stretched region has a size that remains finite even as the overall size of the cone goes to infinity. Thus its size must be of the order of the thickness h of the sheet.

The core region of the d-cone has a crescent shape that is more complex than the core of a simple cone. The crescent has a length comparable to R_* and a transverse width w that appears much narrower than R_*. Moreover, if one examines a d-cone made of ordinary paper, this R_* appears much larger than the thickness. The experimental studies of Cerda, Mahadevan (1998) and Cerda *et al.* (1999) suggested that R_* grows with the ring radius R, and they proposed a scaling argument giving $R_* \sim h^{1/3}R^{2/3}$. Cerda, Mahadevan (2005a) repeat the argument. The argument was based on estimates of bending and stretching energy and on finding an R_* that minimized the total energy. It resembled the argument for the width of a stretching ridge (Lobkovsky *et al.* , 1995; Witten, Li , 1993) to

[2] We use the symbol $\sim$ to mean "scales as". That is, the left and right sides have a finite ratio in the asymptotic limit being considered. The stronger relation "$\simeq$" is defined below.

be discussed below. We now analyze these energies and their implications for R_*, following Liang, Witten (2005). We then review the experimental and numerical findings.

In estimating these, we shall assume that the angular depth $\frac{1}{2}\pi - \beta_0$ of the d-cone is fixed. We shall then vary the elastic thickness h_e defined in Section II and the ring radius R for various assumed choices of the core radius R_*. The actual R_* is that which minimizes the total energy E of Eq. 3. We shall initially suppose that the sheet radius R_p is a fixed multiple of the ring radius R. At the optimal R_* the energy is thus proportional to the bending modulus κ times a dimensionless function of h_e and R. We seek the scaling behavior of R_* in the asymptotic limit $R/h_e \gg 1$.

In considering how R_* influences the energies, it is convenient to imagine building the d-cone in two stages. In the first stage (Liang, Witten , 2005), we remove a small disk of radius R_* to be determined and draw this sheet into the ring, thus forming a truncated d-cone. We denote its energy as E_0. This energy is dominated by bending energy B_e, as in the ideal d-cone: $B_e \simeq \kappa \log R_p/R_*$, as noted above.[3] Though this is the dominant energy in the system, its derivative with R_* is weak and is moreover independent of R. A second exterior stress arises from the tension due to the pushing force. This stress falls off linearly with r like the curvature, and thus the corresponding energy S'_e is logarithmic in R/R_* like B_e. It is weaker (Liang, Witten , 2005) than B_e by a factor of order $(h/R)^2$. Thus it is negligible compared to B_e. Evidently, these exterior energies favor large R_*; they are smaller when R_* is larger. In order to account for the observed scaling of R_*, we must find another contribution to the energy that favors small R_*.

We now transform the truncated d-cone into a d-cone by fastening the core region of the surface back into place. This requires deformation of the inner disk, with its associated energy cost. Closing the surface requires an average curvature of order $1/R_*$, and thus a nominal curvature energy B_c of order $\kappa {R_*}^2(1/{R_*}^2) \sim R_*^0$. The nominal Gaussian curvature in this region is of order R_*^{-2}. As in the spherical-cap example in Section II.A, this leads to an average strain of order unity and thus a stretching energy S_c of order $\kappa {R_*}^2/h^2$. Both of these energies can be qualitatively altered if the curvature varies strongly within the core region. The addition of the core also creates additional forces on the exterior region, and this alters the exterior energy near the core.

Cerda *et al.* (1999) and Cerda, Mahadevan (2005a) p. 697 posit a further stretching energy that couples core and ring radius. It arises from the increase of length of the radial director lines owing to the nonzero size of the core. The authors infer a strain in the sheet by assuming the excess length is distributed uniformly over the sheet. Using this strain, they obtain a stretching energy which allows them to account for the observed growth of R_* with R. However they include only the stretching energy in the core region, omitting the much larger energy that the assumed strain would produce in the exterior region. The justification for this omission remains unclear (Cerda, Mahadevan , 2005b).

We have summarized all the dominant contributions to the energy of both core and exterior regions. Minimizing these energies with respect to R_* leads to the prediction that $R_* \simeq h$ and is independent of R. None of these energies provides a mechanism for the core radius to grow with the ring radius R. On the one hand, the core energies have no R dependence. On the other hand, the exterior energies depend too weakly on either R or R_*. Thus any linkage between R_* and R must come from some subdominant energy too subtle for the estimates above. We shall return to address such subtleties after our discussion of the stretching ridge in Section IV.

D. d-cone experiments and numerics

Many focusing properties of d-cones have been extensively tested and confirmed by experiments and simulations. Numerical solutions of the elastica equations of the preceding section were worked out in connection with these studies (Cerda *et al.* , 1999; Cerda, Mahadevan , 2005a); these give explicit predictions to be tested in experiments. The main experiments were done in Cambridge University, the University of Santiago, Chile and the Ecole Normale, Paris (Cerda *et al.* , 1999; Cerda, Mahadevan , 1998; Chaieb, Melo , 1999; Chaieb, Melo, 2000; Chaieb *et al.* , 1998; Mora, Boudaoud , 2002). . These experiments were complemented by finite-element numerical simulations of elastic sheets (Liang, Witten , 2005).

The experiments confirmed the striking prediction that the buckled region spans an angle $2s_c$ that is a universal number valid for several materials. They verified a prediction that the pushing F varies with the angular depth $\frac{1}{2}\pi - \beta_0$ linearly for small depth and with a fractional power at larger depth. Numerical simulations complement these experiments by allowing one to observe forces and energies that are difficult to measure in an experiment. The simulations of Liang, Witten (2005) approximate the sheet as a triangular lattice of points connected by springs (Seung, Nelson , 1988). The springs are of two types. The first set of springs connects nearest neighbors and provides

[3] We use the symbol $\simeq$ or "about equal" to mean that the ratio of the left to right sides is a finite, pure number in the asymptotic limit of interest. It does not imply that the pure number is numerically close to unity. The weaker relation $\sim$ defined above does not indicate that the ratio is a pure number; it may thus depend on further parameters of the system.

the elastic moduli $\hat{\lambda}$ and $\hat{\mu}$. The second set imposes an energy cost for adjacent triangles that meet at a nonzero angle. This set provides the bending stiffness κ. Thus by varying the ratio of the two spring constants, one may adjust the elastic thickness h_e of the simulated sheet. External potentials are added to account for the pushing force and the ring constraint. For any set of space positions of the lattice points, there is thus a total energy consisting of the external potential and the spring potentials. The equilibrium shape of the sheet in the presence of the external potentials is that which minimizes this total energy. Using standard minimization programs, one may readily determine the shape of a d-cone and the forces and energies within it. This Seung-Nelson sheet has proven useful in other elastic membrane studies to be described below.

The simulations have corroborated the same shape predictions tested by the experiments (Liang, Witten , 2005). Moreover, they quantitatively confirm the localized take-off force, showing that for realistic sheet thickness the peak ring force is orders of magnitude larger than the average ring force.

The experimental studies (Cerda, Mahadevan , 1998; Chaieb *et al.* , 1998) mention in passing that the core radius grows with increasing ring radius R, and propose a power-law form for this increase, as noted above. The chief purpose of the work of Liang, Witten (2005) was to test this prediction. Two different ways of measuring the core radius were completely consistent with the prediction (Cerda, Mahadevan , 1998) $R_* \sim h^{1/3}R^{2/3}$ within the limited range of h and R studied. They were inconsistent with an R^0 or $\log R$ dependence. As noted above, the measurements are thus at odds with expectations based on the dominant energies in the system. We shall return to consider more subtle effects after our discussion of the stretching ridge below.

1. unexpected features

The simulation of Liang, Witten (2005) also uncovered an unexpected departure from the conical shape near the constraining ring (Liang, Witten , 2006). Though the ideal shape has no radial curvature, the real shape must have a radial curvature at the rim. The localized force requires an outward radial curvature of the surface so that the surface elements at the ring may maintain equilibrium. This outward curvature C_{rr} together with the imposed inward curvature of the ring C_{ss} create a Gausssian curvature and thus stretching. The surface must approach the ideal shape as $h \to 0$, and thus the radial angle subtended by the radially curved region must go to zero. However, the curvature C_{rr} need not vanish. Observations of C_{rr} showed a striking regularity. Within the numerical accuracy C_{rr} and C_{ss} are equal and opposite at the ring, so that the mean curvature virtually vanishes there.

The curvature cancellation phenomenon amounts to a new form of spontaneous structure formation in elastic sheets. The numerical studies of Liang, Witten (2006) establish its generality. The two curvatures cancel to roughly one percent precision over a range of thickness and pushing depth throughout the contacting ring, as shown in Figure 10. The numerical data are consistent with complete cancellation at least in the limit $h \to 0$. Though it arises from mechanical equilibrium, the phenomenon is purely geometric: it does not involve material parameters. The effect requires global constraints on the shape. Mechanically, the required radial curvature dictates a specific magnitude of the ring force. This force in turn arises from overall mechanical equilibrium, as discussed above. Empirically, Liang, Witten (2006) found that global changes disrupt the cancellation. If one makes a radial cut before inserting the sheet, the sheet does not buckle and the pushing force is reduced by a factor of order unity. This reduces the ring force and the radial curvature becomes substantially smaller than the transverse curvature. If instead one replaces the d-cone by a real cone, the radial curvature varies widely depending on the pushing force, so the cancellation is in general absent. Likewise, if one replaces the circular ring by an ellipse, the ring force varies with position. Again the cancellation is disrupted. The radial curvature overcompensates the transverse curvature near the minor axis and undercompensates elsewhere.

The curvature cancellation must be compatible with the Föppl–von Karman equations of equilibrium discussed in Section V.A. These equations must thus be able to account for the cancellation effect. Such an accounting must necessarily include stretching effects in the unstretchable limit. It has not been carried out. Moreover, such an accounting would necessarily be mechanical in nature, and thus would give limited insight into this purely geometric phenomenon. Neither is it well-equipped to reveal the generality of the cancellation. The cancellation appears to be a special case of an as-yet unarticulated general property of isometric surfaces.

In this Section we have described unexpected richness in the simple d-cone shape. The universal buckling angle and the sharp take-off force can be understood in the unstretchable limit as a generalization of Euler buckling. However, the anomalous growth of the core radius with the container radius requires a knowledge of residual stretching effects, and remains a mystery. Thus stretching effects appear capable of altering local structure from distant constraints via a mechanism yet to be grasped. A second mystery is the cancellation of curvature at the containing boundary. Some conceptual tools for addressing these mysteries will be shown in the next section on the stretching ridge structure seen in confined sheets.

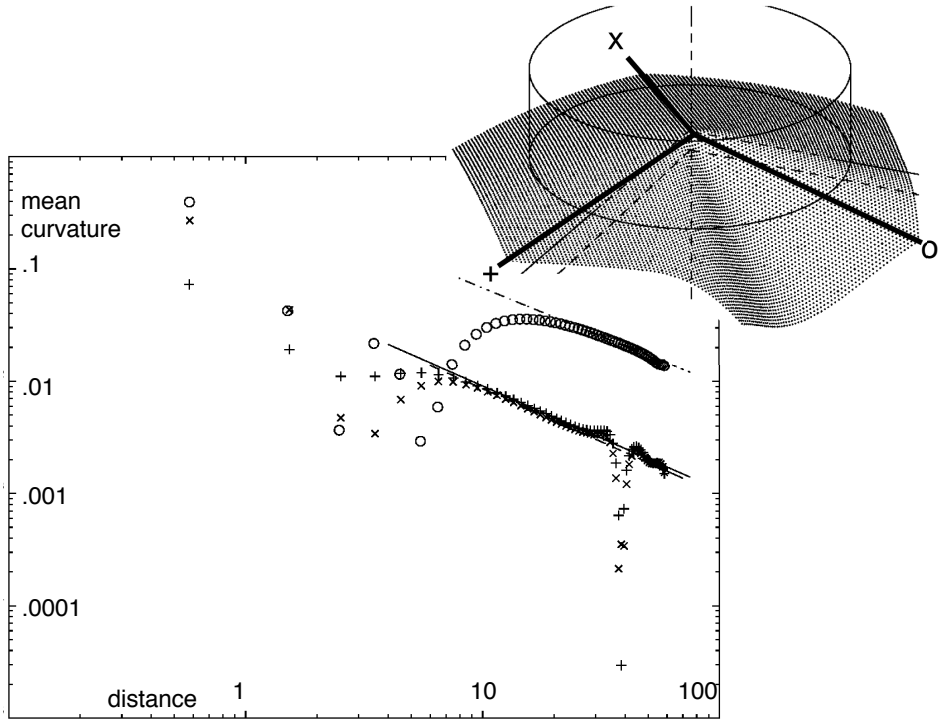

FIG. 10 Log-log plot of mean curvature along three radial lines of the d-cone shown in inset, after Liang, Witten (2006). circles: line in the buckled region, indicated by the heavy line in the inset marked with o. $+, \times$, lines that touch the confining ring, indicated by heavy lines marked with $+$ and $\times$.

IV. STRETCHING RIDGE STRUCTURES

We argued in Section II that when two d-cone-like vertices are present in a sheet, the region on either side of the connecting line must become flat in the unstretchable limit. This entailed a sharp bend along the connecting line, and hence an infinite bending energy relative to the bending modulus. We noted that any finite stretchability would suffice to remove this infinite energy. Thus the actual configuration near this line depends on the degree of stretchability. In this section we explore the interplay of bending and stretching energy that determines this configuration.

As noted in the Introduction, multiple vertices joined by ridges must occur when an elastic sheet is confined within a sphere. The first stage of this process results in a pair of developable cones, as studied by Cerda *et al.* (1999). These authors analyzed the region away from the ridge line and the vertices in the unstretchable limit, as shown in Figure 4. They confirmed that the flanks of the ridge are indeed flat, as anticipated in Section II. They also noted that the flat regions are limited in extent and that part of each d-cone retains its cone-like curvature. We shall reconsider this behavior in Section VI below.

A. variants

Ridges appear to form in a broader class of cases, as illustrated in Figure 11. A simpler variant of the two-d-cone configuration may be made by creating two ordinary cones in a sheet. This is done by removing a wedge-shaped piece of the material from two different places whose vertices are separated by distance X, as shown in Figure 9. When the sides of one wedge are joined, it creates a defect called a disclination. We considered the core region of such a cone in Section III. Now if the second wedge is joined together, the sheet contains two disclinations. Our reasoning from Section II implies that the regions on either side of the connecting line should once again be flat, so that a stretched ridge joining the disclinations should form.

By making multiple disclinations in a flat sheet, one may form a closed polyhedron, as shown in the figure. Such polyhedra provide simplified realizations of interacting ridges and vertices and regions completely bounded by ridges. Another procedure creates ridges in an unbiased way without any imposed inhomogeneity. It consists in joining the opposite edges of a rectangular sheet to form a torus. This constraint creates four symmetrically placed d-cones forming a pillow-like shape.

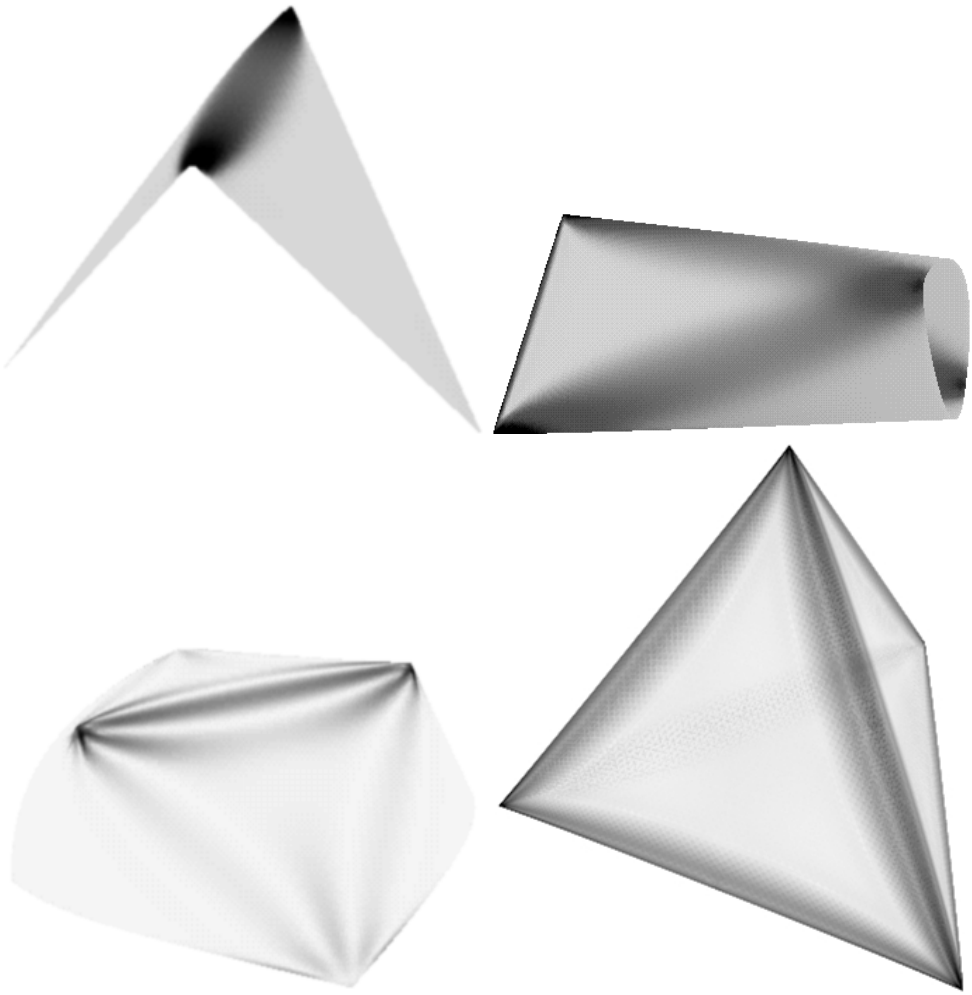

FIG. 11 Simulated configurations showing ridge scaling: kite, bag, boat, after Lobkovsky *et al.* (1995). Kite construction is explained in Figure 12. The bag, boat and tetrahededron are formed by removing sectors from a flat sheet of material and fastening the cut edges together, as implemented in Figure 9. Shading is proportional to local stretching energy density. Alternating bright and dark stripes indicate non-monotonic distribution of energy. The tetrahedron at lower right (DiDonna , 2005) has $h_e/X = 10^{-4}$ and has a ratio of bending to stretching energy $B/S = 5.1$ The simulation has 80 lattice points along the ridge.

A complementary approach makes ridges via smoothly adding boundary forces to a flat sheet. A very tractable example developed by Lobkovsky (1996a) is created by exerting only normal forces. It is called the minimal ridge and is pictured in Figure 13. To form a minimal ridge, one first considers a surface formed by joining two half-planes folded through a dihedral angle 2α. One then introduces a long strip of flat elastic material of width X. Via edge forces normal to the sheet, one then constrains its two long edges to lie in the folded surface. It is apparent from the figure that this smooth procedure creates a ridge region of concentrated bending between the two vertices. As discussed in Section V below, this ridge is amenable to systematic analysis that allows several aspects of its shape and energy to be calculated explicitly.

B. scaling of ridge width

In order to gain a concrete sense of how these ridges form, we consider a further variant called the kite shape. The kite shape is pictured in Figure 12. It consists of a square sheet fastened to a frame at its edges. The frame is hinged so that it can fold along a diagonal, thus forcing the sheet to bend. If one makes such a kite out of *eg.* a piece of office paper stapled into a manilla envelope, one sees that the width of the bent region is significantly smaller than the width of the kite. One also sees directly that the sheet must be stretched. By sighting along the ridge line, one

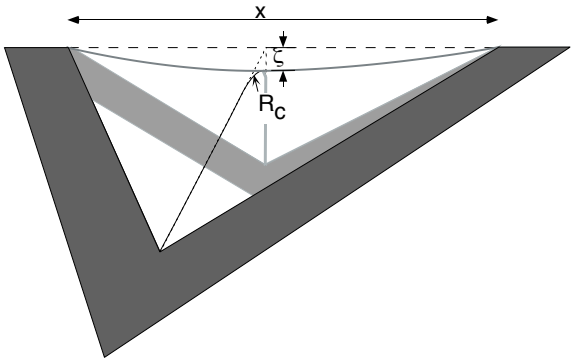

FIG. 12 The kite, a square of elastic material fastened in a hinged frame. Base line is shown as a dashed, horizontal line. The transverse mid-line goes from front to back. This line is the y axis of the material coordinates. The x axis is the ridge line. Ridge length X, assumed curvature radius R_c and sag distance ζ are indicated.

sees a clear sagging of the ridge line. This combines with the transverse bending to form a saddle shape with negative Gaussian curvature. The clear appearance of Gaussian curvature entails stretching.

The sheet is choosing a configuration that minimizes the total of bending plus stretching energy. Clearly stretching is playing a significant role in this energy. For definiteness we now fix the bending angle to some specific value such as 90 degrees. To proceed further we must understand how the geometric constraints lead to a trade-off of bending and stretching energy. We may show this tradeoff by a variational strategy in which we assume a particular shape with a free parameter and then optimize this parameter.

To define this shape, we consider the transverse midline that proceeds from one transverse corner, across the ridge and then to the opposite corner. We define a material co-ordinate x running along the ridge and y running along the transverse midline, as shown in Figure 12. For the moment we shall suppose that this transverse midline retains the same length as in the unbent sheet: it does not stretch. We suppose this line consists of a circular arc of undetermined radius R_c crossing the ridge, connected to each corner by straight segments. It is useful to define the straight line in space between the two ends of the ridge. The unbent sheet passes through this line. We call it the base line and denote its length by X. If $R_c = 0$ the transverse midline also touches the baseline. This forms the sharp bend of an unstretchable sheet. However, if R_c increases from zero, this line with its fixed length cannot reach the baseline. Thus the ridge line must sag below the base line. The distance between the base line and the ridge line is denoted by ζ. If the sheet was bent through angle 2α, then the arc length of half the curved segment is evidently αR_c. This must equal the unbent length. In the limit $R_c \ll X$, the sag ζ must be proportional to R_c, since there is no other length in the system. Specifically, $\zeta = R_c(\alpha/\sin\alpha - 1)$. The bent region has a width $w = 2\alpha R_c$ in the material. We now examine the scaling of the energy with the assumed radius R_c, and fixed α.

The nonzero sag ζ entails that the ridge line must stretch to a length greater than X. Its length has the form $X(1 + \mathcal{O}(\zeta/X)^2)$. Thus there is an average tensile strain γ along the ridge line of order $(\zeta/X)^2$. This strain must occupy the whole region around the ridge line. This region has a width at least of order w, where the bending and hence the sag occur. The associated stretching energy S is proportional to the square of the strain and the elastic moduli. As seen in Section II such moduli are equal up to numerical factors to $\kappa/{h_e}^2$, where κ is the bending stiffness and h_e the elastic thickness. Thus $S \simeq \kappa h_e^{-2} \int \gamma^2$ is of order $\kappa h_e^{-2} w X(\zeta/X)^4$, or $\kappa h_e^{-2} R_c X(R_c/X)^4$. As anticipated, the stretching energy increases rapidly with R_c and thus favors small R_c. By contrast the bending energy B favors weak curvature and large R_c. For $R_c \ll X$ the dominant curvature c is clearly in the transverse direction, with $c \simeq 1/R_c$. The bending region has width of order w and length of order X. Thus $B \simeq \kappa w X c^2 \simeq \kappa R_c X/R_c^2$. This energy varies as $1/R_c$ and thus favors large R_c.

The total elastic energy E is thus the sum of two parts, each varying as a power of our variational parameter R_c. The optimal R_c is that for which $dE/dR_c = dS/dR_c + dB/dR_c = 0$. In view of the power-law form of S, we may write $dS/dR_c = 5S/R_c$. Likewise $dB/dR_c = -B/R_c$. Evidently at the optimal R_c

$$5S = B. \tag{23}$$

This implies a scaling behavior for R_c itself, namely $h_e^{-2} R_c^5 X^{-3} \simeq X R_c^{-1}$, or

$$R_c \simeq X(h_e/X)^{1/3} \tag{24}$$

We see that in the limit $h_e/X \to 0$ our approximation that $R_c \ll X$ is justified.

C. generalization

Though we derived Eq. 23 under restrictive assumptions about the shape of the transverse midline, the result is more general. It requires only that a) the deformed region is confined to a width of the order of the transverse radius of curvature at the ridge, b) the dominant strain is a longitudinal strain confined to a similar region, and c) there is relatively little energy outside this ridge region.

For the kite shape of Figure 12 we may justify assumption c) and thus remove it. This assumption entered our argument through the requirement that the length of the transverse midline be unchanged as the surface was bent. We now allow the midline to stretch. In order to diminish the sag ζ significantly this line must increase its length by an amount of order R_c, incurring a strain of order R_c/X. This strain is larger than the ridge strain calculated above (of order $(R_c/X)^2$. Moreover, it extends over a region much larger than the ridge region. Indeed, it extends over a nonzero fraction of the sheet. Evidently the energy penalty for such stretching is arbitrarily large relative to the ridge energy calculated above. Thus the ridge energy cannot be reduced appreciably allowing strain outside the ridge region, and the assumption c) is justified.

The scaling behavior deduced for the kite shape occurs generally in a line between two vertices. In Section VI we show numerical evidence for a wide range of cases. We also show a formal solution for a tractable geometry that is less restrictive than the kite geometry. We now consider a separate reasoning involving the optimization of Gaussian curvature in order to account for the generality of the ridge scaling. Accordingly, we imagine the region between two neighboring vertices in a crumpled sheet without explicitly considering the surrounding boundaries. We no longer assume the boundary to be clamped. However, we do assume that the strain is confined to the ridge region and that the transverse size of the sheet is of the order of its length X. In this case, the sag ζ inferred for the kite must still be of order of the typical transverse curvature, which we denote $c_\perp$.

The strain induced by the ridge arises from Gaussian curvature. This curvature produces strain as governed by the Gauss fundamental theorem of surfaces. Eq. 11. Disregarding the tensor indices, this equation has the form of the Poisson equation of electrostatics (Jackson , 1999), in which the Gaussian curvature plays the role of a charge density and the strain field plays the role of the electrostatic potential. We may thus view the optimization of the ridge shape as an optimal arrangement of Gaussian curvature in order to minimize the energy. We may begin from the sharply creased surface with no curvature along the ridge line. This configuration has no Gaussian curvature and infinite energy, as noted above.

The Gaussian curvature distribution is limited by a constraint. The Gauss-Bonnet Theorem of Section II dictates that the integral of the Gaussian curvature not change under this optimization, since we are deforming only the interior of the surface. Since the initial state has no Gaussian curvature, the optimal state must thus have equal amounts of positive and negative Gaussian curvature. In view of the behavior of the kite shape discussed above, we anticipate a strip of negative (saddle-like) Gaussian curvature along the ridge line, flanked by strips of compensating positive Gaussian curvature. We denote the width of the whole region of alternating Gaussian curvature as w. We denote its amplitude or typical value by c_G.[4]

With a given bending angle 2α of the ridge, the transverse curvature $c_\perp$ is also constrained. Its integral across the ridge is simply 2α: $c_\perp \simeq \alpha/w$.

Since the Gaussian curvature is proportional to the second derivative of the strain, we expect a typical strain γ of the order of the size of the curved region squared times the Gaussian curvature. The important measure of size is in the direction that determines the second derivative—*i.e.,*the direction of fastest variation. This is the transverse direction of width w. Thus we expect $\gamma \simeq c_G w^2$, and a strain energy $S \simeq (\kappa/h_e^2) w X \gamma^2 \simeq (\kappa/h_e^2) w X c_g^2 w^4$. Similarly, the bending energy B is of order $\kappa w X c_\perp^2 \simeq \kappa w X w^{-2}$. Finally we note that the typical Gaussian curvature is given by $c_G \simeq c_\perp c_\parallel$, and that the longitudinal curvature $c_\parallel$ is given by $c_\parallel \simeq \zeta/X^2 \simeq w/X^2$. Using this relation, we infer $c_G \simeq (1/w)(w/X^2) \simeq X^{-2}$. Thus, we may write the stretching energy as $S \simeq (\kappa/h_e^2) w X (X^{-2})^2 w^4 \simeq (\kappa/h_e^2) w^5 X^{-3}$, as obtained in the kite discussion above. Since S and B vary with the ridge width as in the kite argument above, the optimal width is the same as well.

---

[4] The ridge also imparts a slight bulge to the flank regions beyond the ridge. The Gaussian curvature here is of order $(w/X^2)^2$. The area of the flanks is of order X^2. Thus the flanks contribute an amount of order w^2/X^2 to the Gauss-Bonnet integral. This is much smaller than the nominal contribution of the ridge region, namely $w\ X\ c_G \sim w/X$. Thus we are justified in neglecting the flanks in our optimization.

D. implications

The reasoning above quantifies the focusing of energy at a ridge between two vertices in a simplified geometry. We shall consider in Section VI the generality of this scaling behavior. Here we consider its implications for the overall behavior of the sheet. First, though the predicted structure is sharply bent and strongly stretched on the scale of the whole sheet, it is weakly deformed locally—*i.e.,*weakly strained. The curvature $1/R_c$, while much greater than $1/X$, is nevertheless much weaker than the strong curvature $1/h$ that would lead to nonlinear bending energy. Likewise the strain $\gamma \sim (R_c/X)^2$, while much greater than the strain in most of the sheet, is indefinitely smaller than unity. Thus, even in the limit $h/X \to 0$ of strongest focusing, the predicted local deformation is indefinitely small. That means that the neglect of nonlinear effects in the material in Eq. 3 is justified. This weak strain characterizes the ridge region, though it may not be true of the vertices. The core of the vertex is the site of strongest curvature and strain and some part of the core likely retains a local strain of order unity. This implies that nonlinear effects are not indefinitely small in the core.

The ridge structure predicted above is independent of material. Any solid material obeys linear elasticity under sufficiently small strain. Throughout the region that is significant for the argument, the linear behavior is arbitrarily well obeyed. This means that even a plastic or brittle material, if sufficiently large and thin, must show this ridge structure.

The ridge structure affects the energy of the sheet profoundly in comparison to that of an individual vertex. As noted in Section III, the energy of a vertex grows only logarithmically with the size of the system. When two vertices are present and a ridge forms between them, the energy instead is of the order $\kappa(X/h)^{1/3}$. The energy grows qualitatively faster with the system size than the vertex energy. Thus in the limit, the energy of two vertices is qualitatively larger than that of one. Thus the dominant energy in such a system is the ridge energy. The bulk of the elastic energy in the system occupies an arbitrarily small fraction of the area.

The ridge induces an attraction between the vertices it joins. To see this, we imagine two vertices separated by distance X in a sheet much larger than X. Then evidently the energy in the ridge increases with increasing distance. Thus small distances are energetically favored, and a merger of the two vertices has the lowest ridge energy. On the other hand, the two merged vertices have a larger deformation than either of the constituent vertices, so that the merger carries a cost in vertex energy. One is led to the expectation that weak vertices with a small cone angle $\frac{1}{2}\pi - \beta_0$ tend to attract and form stronger ones, while strong vertices with large cone angles cannot merge and are joined by ridges. Thus *eg.* the boat shape in Figure 11 would have lower energy if the two vertices were brought together, while the bag shape would not, since this would entail infinite energy in the cylindrical flanks of the ridge.

The ridge energy grows slower than linearly with separation X. This means it is unfavorable for a ridge to subdivide into two ridges of length $X/2$.

E. amplitude dependence

Evidently the ridge energy increases from zero as the bending angle 2α increases. We may readily deduce the form of this increase for small α using the scaling analysis above. The angle α enters the energies by constraining the transverse curvature $c_\perp$: $2\alpha = \int dy c_\perp \simeq c_\perp w$. The bending energy B may thus be written $B \simeq \kappa w\ X c_\perp^2 \simeq \kappa w\ X(\alpha/w)^2$. The stretching energy S depends on the sag ζ. For small angle α the analysis above reduces to $\zeta \simeq (1/c_\perp)\alpha^2 \simeq w\alpha$. Using this ζ we infer $S \simeq (\kappa/h_e^2)w\ X(\zeta/X)^4 \simeq (\kappa/h_e^2)w\ X(\alpha w/X)^4$. In the thin limit where $B = 5S$, this implies $(\alpha/w)^2 \simeq \alpha^4 w^4/(h_e^2 X^4)$, so that $w^6 \simeq \alpha^{-2} h_e^2 X^4$. Thus the inverse width increases as the 1/3 power of the angle, and the curvature $c_\perp \sim \alpha^{4/3}$. Finally, the total energy is 6/5 $B \simeq \kappa w X c_\perp^2 \sim \alpha^{7/3}$. The energy increases quite strongly with α.

This analysis gives the behavior of the ridge for small, fixed bending angle in the thin limit $h/X \to 0$. One may also consider the reverse limit, where $\alpha \to 0$ with some fixed, small h/X. Here we must revisit our finding that the ridge energy dominates that of its constituent d-cones. As we found in Section III Eq. 20, the curvature in a cone or d-cone varies as the tangent of the bending angle $\alpha = \frac{1}{2}\pi - \beta$, and is thus linear in α when α is small. The associated bending energy varies as the square of this curvature and is thus quadratic in α. This quadratic dependence dominates the $\alpha^{7/3}$ ridge energy for small α. Thus even for thin sheets the dominance of the ridge energy is not absolute.

In addition to storing energy, the ridge influences the flatter regions on its two flanks. It exerts a tensile stress and a bending moment on these flanks. We may estimate their magnitude by examining a simple case: the region near the transverse midline of a kite bent to an angle of 180 degrees. The boundary tension maintains the constraint that the transverse midline has a fixed length. Thus this tension is needed for the ridge to form. If we relieve the tension, the energy of the ridge relaxes. Using this fact, we may estimate the stress Σ_{yy} via a virtual work argument: $E \simeq X\ \Sigma_{yy}\Delta y$. The displacement Δy is approximately the sag ζ, which scales as w. The energy E of the ridge is of order $B \simeq \kappa w\ X\ w^{-2}$ as found above. From these facts, we infer $\Sigma_{yy} \simeq (\kappa/w^2) \simeq (\kappa/h_e^2)(h_e/X)^{4/3}$. This is the

same order of stress as in a sheet bent to a bending radius w with no ridge. It is a factor of order h_e/w smaller than the longitudinal stress Σ_{xx}. The bending moment imparted to the flanks is also like that of a sheet bent to radius w. These small forces induce a mutual energy to two ridges placed side by side (Lobkovsky and Witten , 1997). In Section V we consider these flank effects in more detail.

F. ring ridge

The ridges seen in confined sheets bear a resemblance to another focused structure seen when cones or spheres are deformed, called a ring ridge. One forms a ring ridge by pushing against a convex shell until a dent is formed. If the shell is thin and elastic, the boundary of the dent becomes arbitrarily sharply curved compared to the radius of the dent. The vicinity of the ring ridge clearly has Gaussian curvature, so that the structure entails stretching like that of the straight ridges treated above. This structure was solved mathematically by Pogorelov (1960, 1988) (Scheidl, Troger , 1987) and further studied by Lobkovsky (1996b).

The same comparison of bending and stretching energies used above may be applied to study the ring ridge. It is simplest to consider a conical sheet which has been inverted in the middle. In the limit of zero thickness, the ring ridge becomes a sharp circular crease of radius R whose circumference $2\pi R$ is equal to that in the undeformed cone. If one gives the ring ridge a nonzero radius of curvature R_c, then the circular ridge line must expand by an amount proportional to R_c, thus creating a strain γ of order R_c/R (compared to $(R_c/X)^2$ for the straight ridge treated above). The strain energy in the ridge region is of order $S \simeq (\kappa/h_e^2)R\ R_c\gamma^2 \simeq \kappa R_c^3/(Rh_e^2)$. The bending energy $B \simeq \kappa R\ R_c R_c^{-2} \simeq \kappa(R/R_c)$. The optimal R_c evidently occurs when $3S = B$, or $R_c \simeq R(h_e/R)^{1/2}$.

The different scalings of the straight ridge and the ring ridge imply qualitatively different asymptotic energies. For a given size $R \simeq X$, the energy of the straight ridge is lower by a factor of order $(h_e/R)^{1/6}$. Thus the straight ridge is more stable. One observes this preference for straight ridges if one creates a ring ridge of a thin material. Unless the amplitude of the dent is very small, the circular ring spontaneously divides into a polygon of straight ridges (Lobkovsky , 1996b).

The scaling arguments of this section revealed an emergent length scale w arbitrarily different from the input length scales h and X of the system. The focusing of stress controlled by this length scale creates the dominant elastic energy in the system. To analyze this focusing more systematically and rigorously is of great interest. In the next section we review such a systematic analysis for the configuration known as the minimal ridge.

V. THE MINIMAL RIDGE

The previous section inferred the characteristic sizes and energies using crude arguments about how the energy varied in a simple class of shapes. Such arguments cannot find the actual shape of minimal energy. Thus they cannot rule out a structure much different from our variational guesses. What is needed is a general variation of shape to determine the shape of minimum energy (Jin, Kohn, 2000; Venkataramani , 2003, 2004) . This state of minimum energy is necessarily a state of mechanical equilibrium of each element of the membrane. The equations for the shape were developed by Foppl (1907) and von Karman (1956) in the early 20th century. Lobkovsky (1996a,b) used these equations to analyze a particular configuration called the minimal ridge. This analysis yielded much explicit information about the ridge shape, as well as a number of unanticipated scaling properties. Our discussion is based on the PhD thesis of Lobkovsky (1996b).

A. Föppl–von Karman equations

In order to determine the equilibrium of a membrane element, we must find the stress and the bending moments everywhere. The Föppl–von Karman method for finding these is a basic element of solid mechanics (Landau, Lifshitz , 1986; Mansfield , 1964). In this section we summarize this method. The bending moments are proportional to the symmetric curvature tensor C_{ij}, as detailed below. This tensor has three independent elements at each point. Likewise, the symmetric stress tensor field Σ_{ij} has three independent elements at each point. These six quantities may be reduced to two via simple geometric and equilibrium conditions.

As noted in Section II, the curvature tensor must obey two differential conditions (Eq. 9) in order to correspond to an unambigouous displacement field $\vec{r}(\underline{x})$:

$$\partial_2 C_{11} = \partial_1 C_{12}, \tag{25}$$

and the analogous relation obtained by interchanging 1 and 2. Imposing these two conditions leaves a single degree of freedom at each point. To identify a suitable degree of freedom, we consider C_{ij} of the form $C_{ij} = \partial_i \partial_j f$ where f

is a scalar function. One readily verifies that an arbitrary f automatically satisfies Eq. 25, Conversely, a $\mathbf{C}$ satisfying Eq. 25 has (do Carmo , 1976) a corresponding "potential"[5] f.

An analogous constraint on $\mathbf{\Sigma}$ arises from the equilibrium of in-surface forces. The equilibrium of forces in the 1 direction implies

$$\partial_1 \Sigma_{11} = \partial_2 \Sigma_{21}, \tag{26}$$

and a second relation obtained by interchanging 1 and 2. Again the tensor field is subject to two differential constraints, and again this allows it to be expressed in terms of a scalar potential, denoted χ:

$$\Sigma_{11} = \partial_2 \partial_2 \chi; \quad \Sigma_{12} = \partial_2 \partial_1 \chi; \quad \Sigma_{22} = \partial_1 \partial_1 \chi; \tag{27}$$

We need only two further conditions in order to determine the potentials f and χ.

One geometric condition about the sheet has not yet been used. It is Gauss's fundamental theorem cited in Section II, Eq. 11

$$c_1 c_2 = 2\partial_1 \partial_2 \gamma_{12} - \partial_1 \partial_1 \gamma_{22} - \partial_2 \partial_2 \gamma_{11} \tag{28}$$

The left hand side is evidently a quadratic function of the curvature potential f, while the right side is linear in the stress and thus linear in the stress potential. The constitutive proportionality constants relating $\boldsymbol{\gamma}$ to $\mathbf{\Sigma}$ are the elastic constants $\hat{\lambda}$ and $\hat{\mu}$ of Eq. 3 . The right side must be a) linear in χ, b) quartic in derivatives, and c) a rotational scalar. Evidently the right hand side has the form $G\Delta^2\chi$, where G is some linear combination of $\hat{\lambda}$ and $\hat{\mu}$. As it happens, the combination G is the Young's Modulus $\hat{Y}$ of Eq. 4.

The form of the left hand side is also strongly constrained by symmetry. It must be a scalar contraction of two second derivatives of f. The combination that emerges is denoted $[f, f]$, where

$$[a, b] \equiv \partial_1{}^2 a \; \partial_2{}^2 b + \partial_2{}^2 a \; \partial_1{}^2 b - 2\partial_1 \partial_2 a \; \partial_1 \partial_2 b \tag{29}$$

Combining, we obtain the "Geometric Föppl–von Karman " equation (Mansfield , 1964):

$$\hat{Y}^{-1} \Delta^2 \chi = -\frac{1}{2}[f, f] \tag{30}$$

To close our system of equations, we require a second relation between χ and f. Such a relation is provided by the equilibrium of forces in the normal direction. Any external pressure P must be balanced by forces in the sheet. If the sheet is curved, the stress $\mathbf{\Sigma}$ provides normal forces. Thus if there is curvature in the 1 direction, the stress Σ_{11} creates normal force. Taking the 1 and 2 directions to be the principal directions for the curvature, the net force per unit area is $C_{11}\Sigma_{11} + C_{22}\Sigma_{22}$. For general orientations, this evidently generalizes to $C_{ij}\Sigma_{ij}$.

Additional forces act on the sheet owing to its bending stiffness. Stresses in the normal direction act on each edge of the sheet element. This stress is denoted Q_1 for the stress acting on the 1 edge and Q_2 for the stress acting on the 2 edge. Uniform Q creates equal and opposite forces on opposite edges and exerts no net force on the element; however, it does exert a torque. This torque must be balanced by the bending moments M_{ij} acting at the edges. For example, M_{11} is a tensile stress at the upper surface and an equal compressive stress at the lower surface, combining to make a torque. Uniform M creates equal and opposite torques at the opposite edges. However, a nonuniform M creates a net torque and thus a Q stress. For example, a gradient of M_{11} requires a nonzero $Q_1 = \partial_1 M_{11}$. A general gradient of M requires a nonzero $Q_i = \partial_j M_{ij}$. If in addition Q varies with position, a normal pressure $\partial_i Q_i = \partial_i \partial_j M_{ij}$ is created. When this source of normal force is combined with the external pressure P and the $\mathbf{C} \cdot \mathbf{\Sigma}$ pressure, the result is

$$\partial_i \partial_j M_{ij} = C_{kl}\Sigma_{lk} + P \tag{31}$$

The linear elasticity of our material assures that $\mathbf{M} \propto \mathbf{C}$, just as $\mathbf{\Sigma} \propto \boldsymbol{\gamma}$. The proportionality constants are linear in the bending stiffness constants κ and κ_G. The components of $\mathbf{C}$ in turn are second derivatives of the curvature

---

[5] The potential f has the dimensions of length. It has a simple interpretation when the sheet is nearly flat and the variation of the normal direction is small. Then it is convenient to represent the distortion of the sheet by giving the normal displacement $h(x, y)$ from the undistorted state. This is called the "Monge representation" (Nelson *et al.* , 1989). For nearly flat sheets the potential f becomes equal to h up to a linear function of position. One readily verifies this by expressing the curvature in terms of h and comparing with the definition of f. When expressed in terms of the full potential f, the Föppl–von Karman equations apply to non-flat sheets. The normal displacement h also obeys the Föppl–von Karman equations provided the sheet is nearly flat, since then h and f become equivalent.

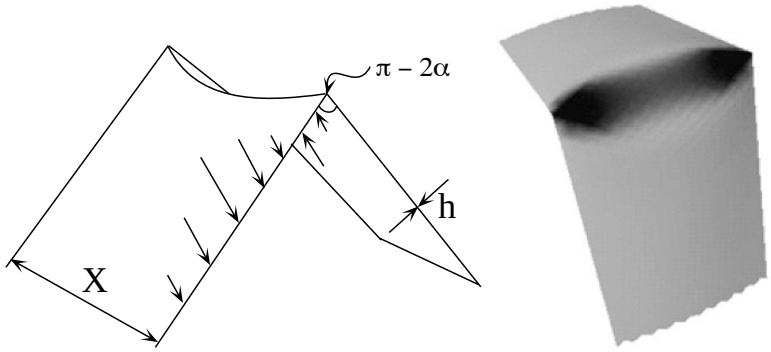

FIG. 13 Two views of the minimal ridge. Left: sketch of the minimal ridge configuration. Normal forces needed to constrain the edges to the frame are indicated. Bending angle α, thickness h and ridge length X are indicated. The positive direction for f and for curvature is downward in this view.

Right: simulation with shading proportional to stretching energy density, after Lobkovsky and Witten (1997).

potential f. Thus, the left side of Eq. 31 must be a) linear in f, b) fourth order in derivatives, c) proportional to some combination of κ and κ_G, and d) a rotational scalar. We have seen that κ_G cannot affect the shape of the sheet in view of the Gauss-Bonnet theorem. The only scalar fourth-order derivative is Δ^2. Thus the left hand side has the form (constant) $\kappa\Delta^2 f$. The right hand side is a scalar contraction of second derivatives of f and χ. The contraction is that of Eq. 29. Combining, we obtain the "Force Föppl–von Karman equation":

$$\kappa\Delta^2 f = [\chi, f] + P \tag{32}$$

The two Föppl–von Karman equations are in principle sufficient to determine the surface. However, their nonlinearity and high order in derivatives make them difficult to exploit. Nevertheless, Lobkovsky (1996a) showed that the ridge scaling of the last section emerges naturally and rigorously from these equations, by analyzing the asymptotic limit of a thin sheet.

B. dimensional simplification

The Föppl–von Karman equations express the competition between bending and stretching energies that controls the shape of the sheet. To show that this competition is controlled by the thickness, we express the variables in appropriate units. We take the bending stiffness κ as our unit of energy. The stress potential χ is an energy and is thus a dimensionless multiple of κ. We express all distances in units of the size X of the sheet. The curvature potential f is then in units of X as well. With this choice of units, in the absence of pressure P the Föppl–von Karman equations simplify to

$$\Delta^2 f = [\chi, f]; \quad \lambda^2\Delta^2\chi = -\frac{1}{2}[f, f], \tag{33}$$

where $\lambda^2 = \kappa/\hat{Y}X^2 = (h_e/X)^2$. We noted in Section II that a typical isotropic elastic sheet has elastic thickness h_e in the range $0.3h$ to $0.33\ h$.

C. boundary conditions for minimal ridge

We have seen that stretching ridges appear when the boundary conditions would impose a sharp crease in the unstretchable limit $\lambda = 0$. The minimal ridge of Figure 13 provides such boundary conditions in a way that is convenient to state in terms of the potentials f and χ. Defining co-ordinates x and y as longitudinal and transverse co-ordinates as before, as $y \to \pm\infty$ the sheet becomes flat and follows its constraining frame; thus it makes an angle α with the horizontal. The sheet normal turns through angle 2α as y goes from $-\infty$ to ∞. Thus $\int_{-\infty}^{\infty} dy\ C_{yy} = 2\alpha$. Recalling that $C_{yy} = \partial_y{}^2 f$, we infer $\partial_y f = \pm\alpha$ for large $|y|$. That is, $f \to \alpha|y|$ for large $|y|$. Along the constraining frame, where $x = \pm\frac{1}{2}$, we have $f = \alpha|y|$ for all y.

The ridge width is expected to shrink to zero with λ. Thus we cannot describe its shape without using co-ordinates that compensate for this shrinkage by changing the scale of y. We do not know in advance how the width behaves.

Thus we define a reduced $\tilde{y} \equiv \lambda^\beta y$, where β is an unknown exponent. When transverse distances expressed in y go to zero, distances expressed in $\tilde{y}$ must remain finite; thus β must be negative. In order for the Föppl–von Karman equations to remain finite as $\lambda \to 0$, we anticipate that f and χ must also be rescaled. The scaling of f must match that of y, since the rescaled description must also describe a ridge of angle α. Thus the rescaled $\tilde{f} \equiv \lambda^\beta f$. The appropriate rescaling for χ is also unknown; thus we use a separate exponent δ to describe it: $\tilde{\chi} \equiv \lambda^\delta \chi$. No rescaling in x is needed, since the dependence on x remains smooth as $\lambda \to 0$.

We must express the derivatives in the Föppl–von Karman equations in these rescaled co-ordinates. All the terms in the derivative $[a, b]$ contain exactly two y derivatives. Thus this derivative in the "$\sim$" coordinates gains a factor $\lambda^{2\beta}$: $[a, b] = \lambda^{2\beta}\ \tilde{[}a, b]$. The Δ^2 derivative is more complicated:

$$\Delta^2 \equiv {\partial_x}^4 + {\partial_y}^4 + 2{\partial_x}^2\ {\partial_y}^2 = {\partial_x}^4 + \lambda^{4\beta}\ {\partial_{\tilde{y}}}^4 + 2\lambda^{2\beta}\ {\partial_x}^2\ {\partial_{\tilde{y}}}^2. \tag{34}$$

As $\lambda \to 0$ the $\lambda^{4\beta}$ term dominates and the others are negligible by comparison.

Expressing the Föppl–von Karman equations in rescaled co-ordinates, we find

$$\begin{aligned} \lambda^{-\beta}\left(\lambda^{4\beta}\ {\partial_{\tilde{y}}}^4\right)\tilde{f} &= \lambda^{\beta-\delta}\ \tilde{[}\tilde{\chi}, \tilde{f}] \\ \lambda^2\ \lambda^{-\delta}\left(\lambda^{4\beta}\ {\partial_{\tilde{y}}}^4\right)\tilde{\chi} &= -\frac{1}{2}\lambda^0\ \tilde{[}\tilde{f}, \tilde{f}]. \end{aligned} \tag{35}$$

With proper choices of β and δ these equations have a finite limit as $\lambda \to 0$. Evidently the powers of λ must cancel on both sides, leading to $3\beta = \beta - \delta$ and $2 - \delta + 4\beta = 0$, or $\beta = -1/3$ and $\delta = 2/3$. The result $\beta = -1/3$ implies that the ridge width scales as $(h/X)^{-1/3}$, in agreement with our initial crude analysis.

This type of asymptotic analysis may evidently be applied to the ring ridge described in Section IV.F above. The appropriate coordinates are polar coordinates. In these coordinates the rescaling introduces additional terms into the derivatives. These additional terms lead to the altered scaling of the ring ridge.

D. ridge shape

The asymptotic Föppl–von Karman equations allowed Lobkovsky (1996a) to infer further scaling properties in the minimal ridge. The arbitrarily slow variation in x compared to that in y led him to postulate that the x position only affects the y dependence through an overall scale factor denoted $q(x)$. That is:

$$\tilde{f}(x, \tilde{y}) = q(x)\ p_1(\tilde{y}/q(x)). \tag{36}$$

Under this assumption every position x has the same $\tilde{f}(y)$ profile except for the scale factor $q(x)$. This $q(x)$ thus dictates the width of the transverse ridge shape at distance x along the ridge. The prefactor $q(x)$ is needed to assure that $\partial_y \tilde{f} = \alpha$ for large y. A similar scaling form is assumed for the stress potential $\tilde{\chi}$: $\tilde{\chi}(x, \tilde{y}) = q(x)p_2(\tilde{y}/q(x))$. Lobkovsky looked for solutions to Eqs. 35 of this form (Lobkovsky , 1996a). In terms of q, p_1 and p_2, these equations (with λ factors removed) may be written

$$\begin{aligned} {p_1}'''' &= q''q^2\left[{p_1}''p_2 + {p_2}''p_1 - \tilde{\tilde{y}}\ ({p_1}''{p_2}' + {p_2}''{p_1}')\right] \\ {p_2}'''' &= -q''q^2\left[{p_1}''p_1 - \tilde{\tilde{y}}\ ({p_1}''{p_1}')\right], \end{aligned} \tag{37}$$

where $\tilde{\tilde{y}}$ denotes the reduced variable $\tilde{y}/q(x)$. The only x dependence in the equations lies in the factors $q''q^2$. The other quantities depend only on $\tilde{\tilde{y}}$. Hence $q''q^2$ must be independent of both x and $\tilde{\tilde{y}}$. We denote this separation constant as A. The width q can readily be computed in terms of this constant. Indeed, the equation $q'' = A/q^2$ has the form of a Newtonian equation of motion in which q is the position, x is the time and $-A/q$ is the potential energy. Following the standard procedure for one-dimensional Newtonian motion, one finds an implicit equation for $q(x)$, *viz.*

$$x = \int^q dQ/|A/Q|^{1/2}. \tag{38}$$

The integral may be expressed in closed form. Now, $q(x)$ must go to zero as x approaches the vertex positions at $\pm\frac{1}{2}$. Using Eq. 38, one readily infers a singular behavior of the width q near a vertex: $q \sim |x - \frac{1}{2}|^{-2/3}$. Evidently the $\tilde{f}$ potential along the ridge line, $\tilde{f}(x, 0)$ shares this singular behavior, as does the sag $z(x)$ of the ridge below the baseline. Thus the shape of the ridge is predicted to have a singular cusp as it approaches either vertex. This singular feature of the ridge shape arises from the inferred scaling form of the minimal ridge, and does not depend on explicit boundary conditions.

The transverse function $p_1(\tilde{y}/q)$ and its counterpart p_2 describing the $\tilde{\chi}$ potential are not as easy to characterize as $q(x)$. The differential equations obeyed by p_1 and p_2 are complicated, and obtaining solutions that satisfy the boundary conditions has proven problematic (Lobkovsky , 1996b). These problems are attributed to a) a breakdown of the scaling form of Eq. 36 for $\tilde{y} \gg q(x)$, or b) corrections to the asymptotic equations Eq. 35. Finding the asymptotic transverse shape of the ridge remains as an unsolved problem.

E. ridge-to-vertex crossover

When the distance $\frac{1}{2} - x \equiv \epsilon$ becomes sufficiently small, one expects the shape to be dominated by the nearby vertex, with little effect from the distant vertex. The crossover from vertex to ridge behavior may be investigated using the Föppl–von Karman equations. The full Föppl–von Karman equations are exact insofar as the membrane obeys the linear elasticity of Eq. 3. Thus they must describe this crossover. However, the asymptotic Föppl–von Karman equations (35) are not exact for small ϵ. Indeed, as $\epsilon \to 0$, the dependence of q on ϵ becomes singular, and so the variation in the x direction is no longer slow compared to that in the y direction. Thus the assumptions made in taking the asymptotic limit no longer apply. Accordingly, we expect corrections to the asymptotic equations to become important for sufficiently small ϵ. We may readily calculate where this crossover occurs. For $\epsilon \ll 1$, the scale factor $q(\epsilon) \sim \epsilon^{2/3}$. We denote the scaled variable $\tilde{y}/q(x)$ by ξ. The reduced function $p(\xi)$ is even about $\tilde{y} = 0$. Using this form of $\tilde{f}$, we readily calculate the leading term in $\lambda^{4\beta}$ and the $\lambda^{2\beta}$ correction. As shown in the Appendix, the range of ϵ where these become comparable is $\epsilon \sim h/X$. This corresponds to a distance $\Delta x = X\epsilon$ from the vertex which is of order h.

By this criterion, the vertex region where the ridge scaling breaks down is confined to a zone whose size is of order h and which thus *remains finite even as* $X \to \infty$. This means that the region near a vertex is qualitatively altered by the creation of a second vertex at arbitrary distance. In Section VI we report a test of this striking prediction.

F. amplitude scaling

The form of the asymptotic Föppl–von Karman equations is independent of the amplitude α. As Lobkovsky noted (Lobkovsky , 1996a), the equations have an exact scaling symmetry under a change in amplitude: if $\tilde{f}(x,\tilde{y}), \tilde{\chi}(x,\tilde{y})$ is a solution, then so is $A\tilde{f}(x,B\tilde{y}), C\tilde{\chi}(x,B\tilde{y})$, where $B^2 = C = A$. This rescaling multiplies the ridge width w by $1/B$ and the ridge angle α by a factor $\partial_{\tilde{y}}\tilde{f}$ or AB. We infer that $w \propto \alpha^{-1/3}$, in agreement with the energy-balance argument of the previous Section. Remarkably this scaling prediction is not restricted to small α.

G. far field

The perturbation caused by a minimal ridge extends for some distance along its flanks. Lobkovsky and Witten (1997) showed that this distance is much greater than the ridge width X. At large distances there is a small but nonzero curvature C_{xx} induced by the distant ridge. This curvature entails a normal displacement $z \simeq X^2 C_{xx}$ along the midline of the flank at $x = 0$. If z is to go to zero at infinity, there is necessarily a curvature $C_{yy} \simeq d^2z/dy^2 \simeq X^2 d^2 C_{xx}/dy^2$. The decay entails Gaussian curvature and thus stretching. The lack of tensile force on the boundaries means that the stretching must occur predominantly in the y direction. The resulting Gaussian curvature induces a strain γ of order $C_{xx}C_{yy}X^2 \simeq C_{xx}X^4 d^2 C_{xx}/dy^2 \simeq z^2/L^2$. The tradeoff between stretching and bending energy is the same as that in a stretching ridge. The imposed curvature entails transverse displacement and induces strain in a long strip of material. The role of the width w is here played by X, while the role of X is played by L. We may repeat the ridge scaling argument of Section IV.B to infer $X \sim L(h/X)^{1/3}$. This flank ridge differs from the main ridge in two respects. a) Any small edge displacement decays in a length of order L, so the decay is exponential. b) The amplitude of the flank ridge goes to zero with h/X, so that its energy E_f becomes a vanishing fraction of the ridge energy E: $E_f \simeq \kappa L X (w/X^2)^2 \simeq \kappa (L/X)(w/X)^2 \simeq E(w/X)$. Unlike the ridge, the flank is fully tractable using the conventional theory of weakly-deformed flat plates (Mansfield , 1964).

H. d-cones revisited

The previous Section on d-cones left a central issue unresolved. We could not account for the length scale of the focusing. There the focusing of stress played only a subordinate role in the energy of the sheet, in contrast to the ridge treated in this Section. Here we saw that when the external constraints dictate regions of nonzero Gaussian

curvature in a sheet, it responds inhomogeneously by making a narrow ridge structure where deformation energy is concentrated. Qualitatively this is the situation at the core of a d-cone. Thus we anticipate that the crescent-shaped core of a d-cone is a type of ridge, whose energy is much smaller than if the Gaussian curvature were spread uniformly over the core radius R_*. Speculating that the crescent has a transverse width (across the crescent, not along it) of order h and that its energy behaves like a ridge, we are led to guess a core energy of order $\kappa(R_*/h)^{1/3}$. It is important to establish whether the focusing of stress in the core indeed behaves like a ridge, a ring ridge, or some new focused structure.

In order to explain the magnitude of R_*, we must understand the coupling of the core region to the constraining ring of radius R. We saw in Section III that the main d-cone energies, present if the core region is cut away, are not sufficient. However, the crescent structure within the core imposes additional forces on the exterior, and these induce energies analogous to the flank energy E_f of the previous subsection. This flank structure is clearly different from the flank of a minimal ridge. In the d-cone case it appears to play a crucial role in determining the focusing length scale. Understanding this structure is an important open question.

This Section has reviewed a rich body of predictions about the focusing properties of stretching ridges. All are predicated in the asymptotic limit in which the sheet becomes arbitrarily thin. In the next Section we review the evidence from numerics and experiments on how well these asymptotic results apply to real sheets of nonzero thickness.

VI. RIDGE SIMULATIONS AND EXPERIMENTS

In this Section we review numerical experiments investigating the ridges discussed above. These experiments can systematically change the elastic parameters and see the resulting structural change. They can also follow aspects of the structure that are difficult for a real experiment to observe, such as the energy distribution. They have explored a great variety of physical situations in order to probe the generality of the scaling laws. They can also test the ideas by examining physically unrealizeable situations like self penetration or high spatial dimensions. On the other hand, they lack several important elements of realism. The experiments only describe ideal elastic material, so they do not include the effects of nonlinear elasticity, plasticity or fracture.

A. numerical methods

All of the various numerical methods discussed here approximate the continuum elastic material as a finite grid of discrete points. The simplest of these is the triangular Seung-Nelson lattice described in Section III. The springs of the lattice impart isotropic in-plane and bending rigidity. The in-plane elasticity gives a Poisson ratio $\nu = 1/3$, so that the elastic thickness h_e is about $0.306h$. With this method, one must assure that the springs are only stretched by a small factor and the angles between adjacent triangles remain small. This requirement dictates a fine lattice spacing and many degrees of freedom near highly curved regions such as a vertex. One may find the minimium-energy state of the Seung-Nelson lattice by simply computing the elastic energy $B + S$ for the initial set of node positions, and then varying these using *eg.* the conjugate gradient algorithm (Press *et al.* , 1992) until a minimum is achieved. In practice for thin sheets, one is led to use elastic thicknesses less than the lattice spacing. Then the minimum-energy configuration is often delicate. That is, the minimization process can lead to a false minimum with unphysical fine structure. To avoid this, one must often resort to decreasing the thickness in gradual increments, of a factor of two or less, so that the initial configuration is not far from the optimal one. One may improve the behavior of the Seung-Nelson simulation in two ways: by using a smoother estimate of local curvature and by using a spatially varying grid spacing (DiDonna , 2001). Alternatively, one may compute the stress and bending moments directly and find the equilibrium state.

These methods have allowed accurate calculations with X/h_e of 10^4 or more. This is a large factor in absolute terms, but in practice it does not give compelling measurements of scaling exponents. For many quantities the regime of small thickness is not reached until $X/h_e > 10^3$. Thus the evidence for power-law behavior with h_e/X covers little more than a single order of magnitude. Such evidence has been sufficient to show consistency with the predictions and inconsistency with qualitatively different alternatives such as logarithmic scaling. More stringent tests would be technically demanding but not unfeasible. The lack of stronger tests to date is due to a lack of alternative predictions to be tested.

B. main scaling predictions

The best-tested prediction from the preceding Section is the magnitude of ridge focusing —that is, the scaling of the relative ridge width w/X or transverse curvature C_{yy} as $(h/X)^{1/3}$. With the limitations stated just above, this

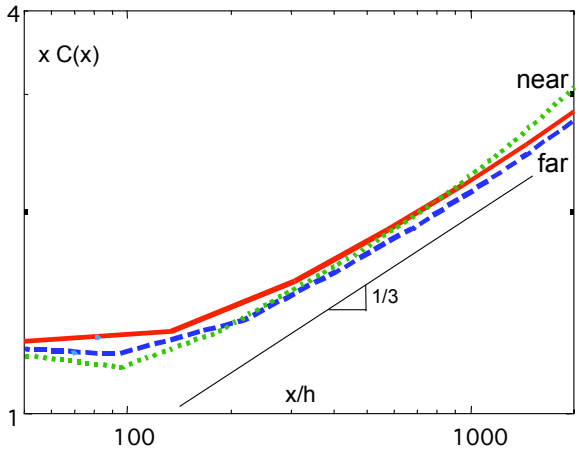

FIG. 14 log-log plot of normalized transverse curvature $x\ C_{yy}$ near a vertex vs distance normalized x/h along a ridge direction of a cube, after DiDonna (2005). The three curves correspond to three different-sized cubes. Top curve at right edge reaches the midpoint of the cube edge. Bottom curve reaches 1/10 of the distance to the midpoint. For an isolated vertex, $x\ C_{yy}$ is independent of x. For a ridge, $x\ C_{yy}$ is expected to scale as $x^{1/3}$.

scaling property has been tested in a wide variety of realizations apart from either the kite or minimal geometry analyzed explicitly above (Chaieb, Melo, 2000). One may join two or more cones to create either open boat or bag structures (Lobkovsky *et al.* , 1995) or closed polyhedra (DiDonna, Witten , 2001; Lobkovsky *et al.* , 1995). For tetrahedra and minimal ridge, the rescaled shape of the ridge transversely and longitudinally has been shown to be independent of thickness, thus supporting the predicted universality. The analytically-predicted shape has further been shown to be consistent with the simulated shape to a few percent precision by simulation (Lobkovsky and Witten , 1997). The scaling with bending angle α has been tested and confirmed for minimal ridges (Lobkovsky and Witten , 1997). Moreover the reduced transverse shape has been shown to be independent of distance to the vertex of a minimal ridge, in support of expectations (Lobkovsky and Witten , 1997). Menon (2005) confirmed the predicted scaling of shape with thickness and bending angle experimentally for a ridge similar to the minimal ridge. The scaling of total energy as $(h/X)^{1/3}$ is more weakly tested. The predicted 5:1 ratio of asymptotic bending to stretching energy was confirmed at the few-percent level, for the particular case of a tetrahedron. Reaching the asymptotic plateau required X/h exceeding 10^4, so that the ridge widths were only a few percent of their lengths as shown in Figure 11. Using such simulations, the total energy could be found explicitly (Lobkovsky , 1996b). When the energy per ridge is expressed in the form $E/\kappa = e\ \alpha^{7/3}(X/h_e)^{1/3}$, then the coefficient e is about 1.2 for the minimal ridge and about 1.16 for the tetrahedron (Lobkovsky , 1996b). Thus the energy appears insensitive to particular boundary conditions.

The striking predictions of remote focusing from the previous Section were confirmed using a simulated cube (DiDonna, Witten , 2001) (DiDonna , 2005). In Figure 14 the curvature at distance x from a vertex is plotted for fixed thickness h and for cubes of varying size. One sees a clear crossover from vertex to ridge behavior. No shift in this crossover is observed as the cube is enlarged by an order of magnitude. It appears that the ridge structure is enforced locally even if the distant vertex that creates the ridge recedes to infinity, as suggested by the Föppl–von Karman analysis of the previous Section.

C. unpredicted features

The numerical experiments summarized above revealed several interesting consequences of ridge formation that were not predicted. Probably the most important is the broad range of applicability. In all cases of two-dimensional sheets where the curvature of a sheet was made to diverge at two points, a stretching ridge with the same scaling properties was observed. This result makes it very plausible that the uncontrolled ridges seen in a crumpled sheet have the same scaling behavior. This supposition leads to strong predictions which will explored in the next Section.

While the scaling of all the ridges studied was consistent with the same law, the pattern of stress and energy within the ridge followed several distinct behaviors, as seen in Figure 11 and 13. The simplest pattern was observed in the minimal ridge, where a monotonic concentration of energy was observed. The strain along the ridge line is compressive in contrast to the kite reasoning of Section IV.B. This compressive stress is supplied by two bands of tensile stress flanking the central ridge line. In the polyhedra examined—tetrahedra and cubes—the transverse bending alternates in sign so that the local ratio of bending to stretching energy alternates as one moves transversely away from the

ridge line.

The open structures tested showed an unexpected secondary focusing at the edge. An example is shown with the bag shape in Figure 11. This shape is a cylinder one of whose ends has been fastened shut, thus forming two disclinations. Each has the same magnitude as in a tetrahedron: the solid angle subtended is 2π. The figure shows four lines of concentrated energy extending from each vertex to two points on the edge where the curvature is strongly concentrated. If this effect were exaggerated further, the final shape would approach that of a closed tetrahedron.

Some insight into the reason for this induced focusing comes from the Cerda *et al.* (1999) study of d-cone pairs in the unstretchable limit. Here they reported a numerical study of a surface forced into a circular constraint by two point forces. A sharp ridge flanked by flat facets formed, consistent with the arguments of Section II. However, these two facets do not extend to include the whole sheet. Instead, each flat region is confined to an isosceles triangle connecting the vertices to the edge as shown in Figure 4. Beyond these two triangles, the surface is no longer flat. The straight directors converge to the nearest vertex, and remain unaffected by the other vertex. It appears that flatness is only required for points equidistant from the two vertices and the directors from such points to these vertices. The remote focusing of curvature to points on the boundary is another aspect of stress focusing that remains to be understood.

D. higher dimensions

We saw in Section II that the basic conditions leading to stress focusing exist not merely for two-dimensional sheets but for higher dimensions as well. We found that strictly unstretchable sheets are not confinable to volumes indefinitely smaller than the resting size of the sheet. Thus any real sheet when so confined must stretch. Since uniform stretching costs more energy than localized ridge-like stretching, one expects focusing in such cases. This is expected whenever a manifold of m dimensions is confined in a space of less than $2m$ dimensions. However, the nature of the confinement and localization is ill-understood. The possibilities for bending, twisting and stretching are clearly much increased in high dimensions. Thus the potential for new forms of stress focusing is correspondingly great. In this section we review the existing numerical information about the nature of this focusing.

Representing an m-dimensional elastic manifold numerically is not as difficult or ambiguous as one might imagine. It suffices to create a d-dimensional lattice of springs with a large extent in m dimensions and a small thickness h in the remaining $d-m$ dimensions. The energy of deformation is thus the energy in the springs. In continuum language, the local distortion is expressed as a second-rank d-dimensional strain tensor γ_{ij} defined by Eq. 12. If the material is isotropic, the associated energy has the form $S[\boldsymbol{\gamma}]$ given in Eq. 3. Thus no new parameters are needed to define an elastic manifold of general dimensions. As with two-dimensional sheets, we may represent the deformation more economically via an m-dimensional strain tensor $\boldsymbol{\Gamma}$ and a curvature tensor (do Carmo , 1976) (Kramer , 1997). For any given normal direction α one may define a curvature tensor element $C_{ij}{}^{(\alpha)}$ for any two directions i and j in the manifold. The elastic energy is then a simple quadratic form in $\boldsymbol{\Gamma}$ and $\mathtt{C}$. One may readily determine and minimize this energy for an m-dimensional lattice of springs, in analogy with the method of Seung, Nelson (1988). It is this numerical implementation that was used for the results reported below. We may also use this energy to anticipate the nature of the focusing, even without knowing an analog of the Föppl–von Karman equations.

To anticipate what focusing might occur when such a manifold is confined, we first try to follow our previous reasoning. Section II anticipated that vertex structures should exist in general manifolds. These are internal boundaries in the manifold where unbent director lines converge. In a two-dimensional sheet ridges form because of the joint effects of two such vertices. The joint requirements on the directors leading to both vertices entails that all curvature must vanish. The arguments for two-dimensional sheets are applicable whenever the curvature is described by a second-rank tensor on the manifold. However, for higher embedding dimensions such a tensor is not sufficient to specify the state of bending as noted above. For example a one dimensional curve in three dimensions needs two quantities to specify the curvature at each point. There is no clear notion of principal curvatures in general, and thus the argument leading to zero curvature has no clear counterpart. Thus we many anticipate ridge-like structures when $d = m+1$, but for $d > m+1$ it is unclear whether any focused structure other than the vertices of Section II.C occurs.

We can readily describe the degree of focusing caused by vertices in higher dimensions in a unified way. As discussed in Section II.C, each vertex is a set of points in the manifold onto which straight director lines converge. For example if the embedding dimension d is $2m-1$, the vertices are isolated points, as in a 2-sheet in three dimensions. Director lines converge onto these points from the surrounding sheet. This leads to curvature of order $1/r$ for points at distance r from the vertex. [6] The bending energy density $b(r)$ there is thus of order $1/r^2$. Within a volume V of order r^m

[6] To see that points at distance r near a vertex have curvatures of order $1/r$, consider two director lines A and B meeting at the vertex

one thus has a bending energy density of order $V^{-2/m}$ or greater. As in an ordinary cone, the nonuniform bending moment gives rise to a stress of order $1/r^2$. The stretching energy density $s(r)$ is proportional to the square of this stress, and thus to $1/r^4$. For distances $r \simeq h$, bending and stretching are comparable. Thus the stretching energy s at a given point can be related to b there by $s \simeq s(h)(b/b(h))^2$. Thus for very thin sheets s becomes increasingly unimportant and bending dominates, so that the energy is well-defined in the unstretchable limit.

By contrast, when ridges are generated, the system requires a balance of bending and stretching energy, and the two forms of energy remain comparable. For ridges of length X each energy is confined to a fraction w/X of order $(h/X)^{1/3}$ with an energy density of order $1/w^2$. We saw in the last subsection that for distances $r \ll X$ from a vertex, X becomes irrelevant and $w \simeq r(h/r)^{1/3}$. Thus near the vertex there is a concentration of energy density. We now consider a two-dimensional section of the manifold intersecting the two vertices and the ridge connecting them[7]

The area $A(b)$ that has energy density b or greater is roughly $r\ w$. Using $b \simeq w^{-2}$ and $r \simeq w^{3/2}h^{-1/2}$, we infer $A(b) \sim b^{-5/4}$. The fraction of the system with energy density exceeding b goes as $b^{-5/4}$. Conversely, for some given fraction ϕ of the system the bending energy density exceeds some $b(\phi)$. This "energy density profile" tells how strongly the energy is concentrated. It is a useful way to quantify energy focusing, since it does not require a knowledge of where the focusing occurs. Thus according to the reasoning in this paragraph, a ridge should have have $b(\phi) \sim \phi^{-4/5}$. Since bending and stretching energies are comparable in a ridge, the stretching energy profile $s(\phi)$ must fall off with increasing ϕ in the same way. These features of the energy density profile should not change their form when one increases the size of the system or if it includes multiple ridges or vertices.

Didonna, Venkataramani, Witten and Kramer (DiDonna *et al.* , 2002) explored numerically the condensation of energy of several kinds of two- and three-dimensional sheets embedded in 4, 5, and 6 dimensional space. For each example they determined the profile of stretching and bending energy density. A representative sample appears in Figure 15. The system was a three-dimensional cube embedded in higher dimensional space, with the three pairs of opposite faces joined to form a torus. In six dimensions, the torus is smooth and the energy density is uniform. In five and four dimensions, points of high energy form. Though no qualitative difference is apparent in the pictures, the profiles show a clearcut difference. In five dimensions, the stretching energy falls off as roughly the square of the bending energy. The bending energy itself falls off roughly as $\phi^{-2/3}$, as anticipated above for pointlike vertices in a three-dimensional manifold.

By contrast, the profile in four dimensions shows a rough proportionality of bending and stretching energy. Moreover, the density falls off with ϕ roughly as $\phi^{-4/5}$. The profile thus behaves like the predicted and measured profile of a two-dimensional sheet in 3 dimensions showing a ridge. The pictures support this view, showing flat surfaces of high energy density corresponding to the ridge regions.

All of the shapes studied showed one of these two behaviors. Taken together, these examples suggest that constrained m-dimensional manifolds create stretching ridges that dominate the energy when embedded in $m+1$ dimensions. However in higher embedding dimensions, the energy focusing is consistent with directors converging towards vertices. Here the energy is dominated by bending and is as expected in an unstretchable sheet. Unlike the ridge case, the stretching that occurs in the vertices makes a vanishingly small contribution to the energy.

VII. INTERACTING VERTICES AND RIDGES

When a large sheet is crushed into a small volume, the pattern of ridges and vertices is rich and stochastic. In this Section we review the behavior of these systems of many foci of energy and stress. The response of simple systems to controlled forces has been measured in a variety of contexts. Numerical and physical experiments have also revealed regular scaling behavior in crumpled sheets with many foci.

---

and the two-dimensional submanifold containing them. Every point in this submanifold belongs to a director that also meets at the vertex. In general the director C through a given point is not coplanar with the original directors A and B. Thus the directors A, B, and C span a three-dimensional subspace in which the two-dimensional manifold is isometrically embedded. This submanifold must follow the familiar behavior of a 2-sheet in 3-space, in which the curvature is of order $1/r$.

[7] The choice of such a section is not very restrictive. We first suppose that the whole manifold has only two vertices. As noted above, we anticipate ridges only when the embedding dimension d is $m+1$, so that the vertices must have dimension $m-2$. Thus generic two-dimensional sections of the manifold would intersect each vertex at a point. Now if the manifold contains many vertices separated by distances of order X, then a typical two-dimensional section that lies within distance X of two vertices should intersect each at a point.

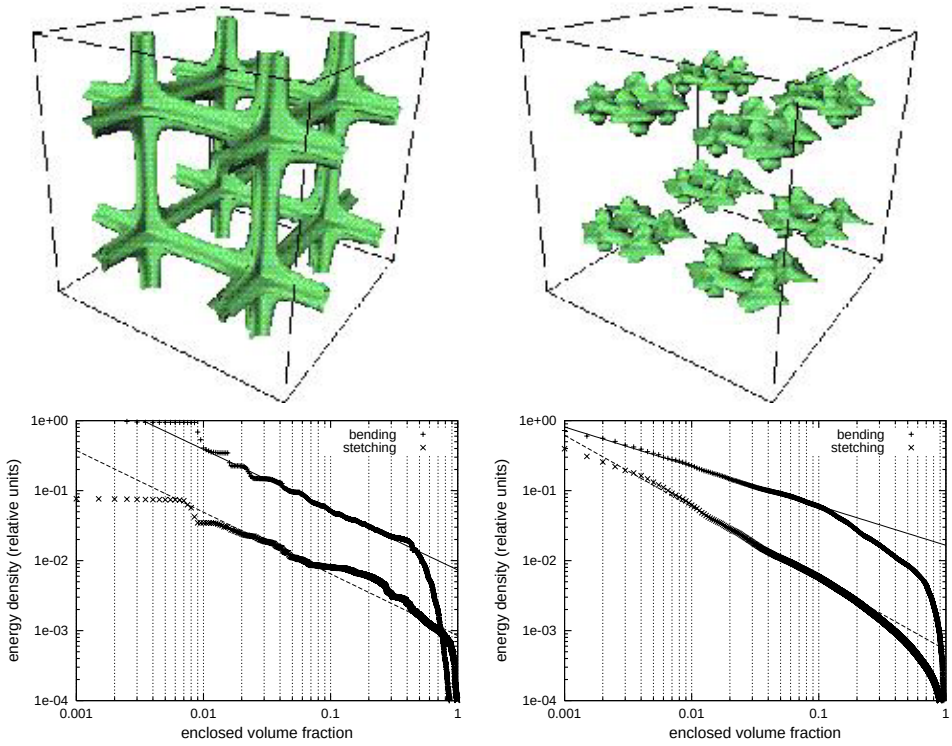

FIG. 15 Energy density profiles for a simulated elastic cube with opposite faces joined to make a torus, embedded in 4 dimensions (left) and 5 dimensions (right), after DiDonna *et al.* (2002). Upper pictures show the material co-ordinates with the 2.5 percent of the volume with highest density indicated. Log-log plots show the corresponding energy profiles. Upper curves are bending energy density; lower curves are stretching energy density.

A. vertex interactions

Boudaoud *et al.* (2000) studied the effect of a point force on a cylindrically bent sheet. The indentation caused by the point force creates a pair of vertices. With increasing indentation these vertices rotate around the pushing point. This shows that external forces create organized movement of the focused structures. Hamm *et al.* (2004) extended this study greatly by imposing axial torques on a thin cylinder. He found that the vertices thus produced follow laws of climb and glide similar to that of dislocations under stress (Landau, Lifshitz , 1986). However, the mechanistic reason for this parallel is not understood.

B. ridge interactions

In order to find the mutual influence of two ridges, Lobkovsky and Witten (1997) created two parallel minimal ridges in a sheet and measured how the total energy varied with distance. They found that the bulk of the interaction energy falls off on the scale of the ridge width. However, a small interaction must persist to very long distances owing to the flank energy treated in Section V.G. In the cases treated numerically with $X/h \simeq 10^3$, this long-range part was too small to be visible. In the polyhedra of Lobkovsky *et al.* (1995) and in real crumpled sheets, the ridges likely exert tensile forces on one another and thus probably to reinforce one another. We know of no direct measure of this effect.

C. ridge buckling

We have noted that ridges of a given size typically contain qualitatively more energy than do cones or d-cones of that size. Thus the work required to deform a surface is large if the deformation creates ridges. Large work of deformation

amounts to mechanical strength. One may test this strength directly by exerting external forces on a ridge-containing structure. DiDonna, Witten (2001) measured this strength numerically using a simple ridge-containing structure, a cube. They studied the deformation under small forces and the force required to buckle the cube. Both of these responses were as one would anticipate in terms of the ridge energy. The added force increased the sag of the ridges, and the increased ridge energy was proportional to the increased sag. Buckling occurred when the added work of compression was a fixed multiple of the ridge energy. They were able to account for both the buckling force and the position of buckling by treating the ridge as locally cylindrical and using the conventional analysis for cylinders (Thompson *et al.* , 1984). The buckling was abrupt and discontinuous (*i.e., subcritical*), so that a fixed fraction of the energy was lost upon buckling. This occurred even when the cube was deformed with fixed displacement rather than fixed forces.

DiDonna (2002) explained several features of the buckling by treating the ridge as a nearly cylindrical shell of radius w. The abruptness of the buckling was a natural outcome of this analysis. The buckling occurs in a local region. The loading of this region comes from two slender adjoining regions in compression. The elasticity of these regions effectively supplies fixed force to the buckling region. Even though the overall system has fixed displacement, the buckling region experiences nearly fixed force. This becomes more nearly true as the sheet becomes thinner. As with a thin cylinder, the buckling under fixed force is subcritical (Thompson *et al.* , 1984).

Buckling cylinders do not require internal stress for their buckling strength. The strength is comparable whether they are made from flat material thus creating internal stress or whether the stress is relaxed in the cylindrical state. The same proved to be true with the cubes. To test this, the springs in the lattice making up the cube were adjusted after the cube was formed, so that the springs were all relaxed and no energy was stored. Nevertheless the stiffness and buckling strength were virtually unaltered. Evidently the energy to deform an existing ridge or buckle it is comparable to the energy to make it from a flat sheet, even if one removes that initial energy.

D. crushing energy

The work to compress a thin sheet into a small volume is equal to the energy of deforming it. For a sufficiently thin sheet, we have shown above that the bulk of this energy goes into creating stretching ridges. Most of this energy is expected to be in ridges of large bending angle α. Then the work W to compress can be readily related to the lengths X_i of these ridges. Up to numerical constant, the work W is given by $\sum_i \kappa (X_i/h)^{1/3}$.

Numerical and physical experiments have been done to find the work of compression. Kramer, Witten (1997) compressed a hexagonal Seung-Nelson sheet inside a repulsive spherical potential. The sheet had no constraints against self-penetration. The range of compression was small and didn't permit a clear test of energy scaling. However it showed clearly that the ridges created were at the length scale of the container. It also showed that the system became more homogeneous with greater compression, and the fluctuations of energy from run to run became smaller.

The work to crush a given type of sheet is of great importance for practical purposes. Still, there has been little attention given to finding systematic scaling behavior with thickness and compression factor. Recently such a test using mylar plastic sheets was done by Nagel and co-workers (Matan *et al.* , 2002). The sheets were crushed in a cylindrical piston and the volume versus force was measured. Several unanticipated stress relaxation and history-dependent effects were discovered. Ultimately a robust power-law relationship was found between force and compression. The experiment was done in the range of large compressions where X_i/h is not large and the approximation of a thin sheet is only qualitatively applicable.

By using the relation $W \simeq \kappa \sum_i (X_i/h)^{1/3}$ one may anticipate the behavior of the sheet. For this it is necessary to estimate the ridge lengths X_i. A natural approach is to assume that a) the X_i are roughly equal and b) the typical size X is that size that would fill the allowed volume without strong mutual intersection effects. We can readily estimate this size X. If the sheet of linear size L is dispersed into N small sheets of size X, then the sheets may rotate without mutual interference if each is allowed to occupy a volume X^3 or more. Since $N \simeq (L/X)^2$, the total volume thus occupied is of order $V \simeq NX^3 \simeq L^2 X$. Evidently this volume may be made smaller than the confining volume V by making $X \lesssim V/L^2$. The least energy that avoids mutual interference gives $X \simeq V/L^2$. This gives an energy W of order $\kappa N (X/h)^{1/3} \simeq \kappa L^2 L^4/V^2 (V/(L^2 h))^{1/3}$. Defining the occupied volume fraction $V/(L^2 h) \equiv \phi$, this gives

$$W/V \simeq \kappa h^{-3} \phi^{8/3}. \tag{39}$$

The corresponding pressure is 5/3 W/V and also varies as $\phi^{8/3}$. The predicted pressure increases strongly but smoothly over a wide range of density. For comparison we note that the osmotic pressure of a conventional polymer solution varies as $\phi^{9/4}$ (deGennes , 1979)

The strongly compressed sheets of Matan *et al.* (2002) have a pressure that is smaller and more slowly growing with density than this estimate gives. Possible reasons for this discrepancy are plastic deformation in the sheet and

alignment of the ridge elements, thus allowing them to be larger and less numerous. Friction between contacting facets is also neglected in the estimate. Such friction should increase the strength.

E. heterogeneity and complexity.

Real sheets appear to be qualitatively more heterogeneous than the phantom computer sheet of Kramer, Witten (1997). If one views a crumpled sheet such as Figure 1, one sees ridges spanning a wide range of size scales. Such heterogeneity arises naturally if one views the crumpling as a repeated buckling process. Upon compression each ridge buckles to form a small number of different-sized sub-ridges. Further compression causes these in turn to buckle. Such processes give a broad distribution of final sizes. To show this in a simple way, we consider a stick that is broken into a large segment and a small segment that is x times the original size. Now the two pieces are each divided into uneven sub-pieces in the same proportions. The breaking continues for a large number of stages k. Now we choose a piece at random. The length of this piece is the product of k factors, each of which is either x or $1-x$ with equal probability. These factors are random and independent since each refers to a separate random breaking event. Since the length is the product of random factors, the log of this length is the sum of random terms. Thus the logs of the lengths are approximately normally distributed. The lengths themselves have a log-normal distribution. For a wide range of L values, such log-normal distributions behave approximately as $1/L$. The same reasoning applies to any power of L. All such quantities have a power-law falloff with an apparent exponent near -1.

Recently Sultan, Boudaoud (2006) showed how such heterogeneity could arise from a non-hierarchical description. their numerical approach seeks configurations that obey the constraints of confinement and self-avoidance with a minimal degree of buckling. They simplify to a one-dimensional line that is allowed to bend only at discrete points. They explore the effects of confinement, extending to a maximum density. At high confinement with many bends but far below the maximum density they observed a log-normal distribution, though no hierarchical breaking is explicitly performed.

Indirect evidence in favor of this log-normal distribution comes from measurements of the sound(Gopinathan *et al.* , 2002) of crumpled sheets (Houle, Sethna , 1996; Kramer, Lobkovsky , 1996). These studies recorded the crackling sounds of crumpled sheets and compiled the probability distribution of acoustic energies e in a sound burst. The distribution $P(e)$ is approximately proportional to $1/e$, and the departures from this power law resemble those expected for a log-normal distribution. Recently a direct measurement of ridge lengths (Blair, Kudrolli , 2005; Vliegenthart, Gompper , 2006) also shows log-normal-like behavior.

The hierarchical buckling mechanism is a kinetic one, and not one that selects the lowest-energy state. Its success leads us to ask what aspects of crumpled structure might be kinetic and what aspects have minimum energy. One way to explore this issue was done in an insightful study by Menon (2005). In this study a sheet was crumpled gradually so that the individual buckling events could be followed. If these events occur in a hierarchical sequence, one might suppose that reversing the compression might simply reverse the sequence. Alternatively, it could be that reversal of compression would send the system along a new path, so that repeated compression and decompression explores an extended ensemble of states. The experimental results appear to favor the extended-ensemble picture.

Blair and Kudroli did extensive measurements of the statistical properties of crumpling by studying the topography of uncrumpled sheets. Residual plastic deformation left traces of the ridges and vertices in the previous crumpled state. They measured the probability distribution of curvature and found it to be exponential. This probability distribution corresponds closely to the $\phi(b)$ function defined in the previous Section. There we saw that this function is a power law for a single ridge, rather than an exponential. The study measured the connectivity of the ridge network and found many disconnected ends. The crumpling of real sheets clearly has many unexplained features.

VIII. CONCLUSION

Physical science has come to recognize an increasing range of self-organizing mechanisms by which matter comes to be spontaneously structured. Spontaneous symmetry breaking of spatially distributed fields in thermal equilbrium (Stanley , 1987) is a major source of such structure. More recently stochastic growth phenomena (Vicsek , 1992) have shown robust fractal structure. Certain kinds of nonlinear deterministic dynamics lead to the intricate patterns of chaotic systems (Ott , 2002). The flow of fluids with inertia (Davidson , 2004), hydrodynamic interactions (Ramaswamy , 2001) and capillary forces (Eggers , 2005) lead to further varieties of structure. In this paper we have seen that stress focusing can give forms of self-organization that are independent of these better-studied forms. It creates robust and universal structures such as stretching ridges and d-cones. These structural elements interact to create further levels of structure such as induced vertices and crumpled sheets that are little understood at present. These are particularly simple forms of emergent structure, since the only requirement for their creation is an elastic

sheet—a manifold with a metric. For this reason they may offer a hint into the deeper origins of structure formation in locally-coupled matter.

Acknowledgments

The author is grateful to Brian DiDonna for providing unpublished data showing remote focusing. He warmly thanks Alex Lobkovsky, Eric Kramer, Shankar Venkataramani, Tao Liang, Sidney Nagel, Narayanan Menon, Enrique Cerda, L. Mahadevan, and Arezki Boudaoud for many instructive discussions.

References

Albuquerque, R. F, and M. A. F. Gomes, 2002, Physica A **310** 377.
Audoly, B., 1999, Phys. Rev. Lett. **83**, 4124.
BenAmar, M., and Y. Pomeau, 1997, Proc. Royal Soc. Lond. A **453**, 729.
BenAmar, M., and Y. Pomeau, 1998, Phil. Mag. B **78**, 235.
Belgacem, B. H., S. Conti, A. DeSimone, 2002, Archive For Rational Mechanics and Analysis **164** 1.
Belgacem, B. H., S. Conti, A. DeSimone, and S. Muller, 2000, Journal of Nonlinear Science **10** 661.
Blair, D. L., and A. Kudrolli, 2005, Phys. Rev. Lett. **94**, 166107.
Boudaoud, A., P. Patricio, Y. Couder, and M. BenAmar, 2000, Nature **407**, 718.
Boudaoud, A. S., and S. Chaieb, 2001, Phys. Rev. E **64**, 050601.
Bowick, M. J., and A. Travesset, 2001, Phys. Reports **344**, 255.
Cerda E., S. Chaieb, F. Melo, and L. Mahadevan, 1999, Nature **401**, 46.
Cerda, E., and L. Mahadevan, 1998, Phys. Rev. Lett. **80**, 2358.
Cerda, E., and L. Mahadevan, 2003, Phys. Rev. Lett. **90**, 074302.
Cerda, E., and L. Mahadevan, 2005a, Proc. Royal Soc. Lond. A, **461**, 671.
Cerda E., and L. Mahadevan, 2005b, private communication.
Cerda, E., L. Mahadevan, and K. Ravi-Chandar, 2002, Nature **419**, 579.
Chaieb, S., and F. Melo, 1997, Phys. Rev. E **56**, 4736.
Cohen, I., and S. R. Nagel, 2002, Phys. Rev. Lett. **88**, 074501.
Chaieb, S., and F. Melo, 1999, Phys. Rev. E **60**, 6091.
Chaieb, S., and F. Melo, 2000, J. Mech. Phys. Solids **48**, 565.
Chaieb, S., F. Melo and J. C. Geminard, 1998, Phys. Rev. Lett. **80**, 2354.
Conti, S., A. DeSimone, and S. Muller, 2005, Computer Methods In Applied Mechanics and Engineering **194**, 2534.
da Silveira, R. , S. Chaieb, L. Mahadevan, 2000, Science **287** 1468.
Davidson, P. A., 2004, *Turbulence: An Introduction for Scientists and Engineers*, (Oxford University Press, New York, USA).
DeArcangelis, L., A. Hansen, H. J. Herrmann, et al, 1989, Phys. Rev. B **40** 1.
Debregeas, G., P. G. de Gennes, F. Brochard-Wyart, 1998, Science **279** 1704.
DeGennes, P. G., 1979, *Scaling Concepts in Polymer Physics*, (Cornell University, Ithaca, New York).
DiDonna, B. A., 2001, (PhD thesis (University of Chicago)).
DiDonna, B. A., 2002, Phys. Rev. E **66**, 016601.
DiDonna, B. A., 2005, private communication.
DiDonna, B. A., and T. A. Witten, 2001, Phys. Rev. Lett. **87**, 206105.
DiDonna, B. A., S. C. Venkataramani, T. A. Witten, and E. M. Kramer, 2002, Phys. Rev. E **65**, 016603.
do Carmo, M., 1976, *Differential Geometry of Curves and Surfaces* (Prentice Hall, Englewood Cliffs NJ).
Eggers J., 2005, Zamm-Zeitschrift für Angewandte Mathematik und Mechanik **85**, 400.
Eisenhart, L. P., 1909, *Differential Geometry*, (Ginn and Company, New York).
Euler, L., 1736, *Mechanica, sive motus scientia analytice; expasita*, (Ex Typographia Academiae Scientiarum, A, St Petersburg, Russia)
Foppl, A., 1907, *Vorlesungen uber Technische Mechanik V*, (Teubner, Leipzig) pg. 132-144.
Fournier, J. B., and E. Virga, 1996, Proc. Royal Soc. Lond. A **452**, 1251.
Ganan-Calvo A. M., 1998, Phys. Rev. Lett. **80** 285.
Gopinathan, A., T. A. Witten, and S. C. Venkataramani, 2002, Phys. Rev. E **65**, 036613.
Guitter, E., F. David, S. Leibler, and L. Peliti, 1989, J. Phys. (Paris) **50**, 1787.
Gyure, M. F., and P. D. Beale, 1992, Phys. Rev. B **46(7)**, 3736.
Hamm E., B. Roman, and F. Melo, 2004, Phys. Rev. E **70**, 026607.
Houle, P.A., and J. P. Sethna, 1996, Phys. Rev. E **54**, 278.
Jackson, J.D., 1999, *Classical Electrodynamics, 3rd Edition*, (Wiley & Sons, New York).
Jin, W., and R. V. Kohn, 2000, J. Nonlinear Sci. **10**, 355.
Kergosien Y. L., H. Gotoda, and T. L. Kunii, 1994, IEEE Computer Graphics And Applications **14**, 40.
Kramer, E. M., 1997, J. Math. Physics **38**, 830.
Kramer, E. M., and A. E. Lobkovsky, 1996, Phys. Rev. E **53**, 1465.

Kramer, E. M., and T. A. Witten, 1997, Phys. Rev. Lett. **78**, 1303.
Landau, L. D., and E. M. Lifshitz, 1986, *Theory of Elasticity, 3rd Edition*, (Pergamon, New York).
Nelkin, M., 1992, Science **255**, 566.
Liang, T., and T. A. Witten, 2005, Phys. Rev. E **71**, 016612.
Liang, T., and T. A. Witten, 2006 Phys. Rev. E **73**, 046604.
Lobkovsky, A., S., Gentes, H. Li, D. Morse, and T. A. Witten, 1995, Science **270**, 1482.
Lobkovsky, A. E., 1996a, Phys. Rev. E **53**, 3750.
Lobkovsky, A. E., 1996b, (PhD thesis (University of Chicago)).
Lobkovsky A. E., and T. A. Witten, 1997, Phys. Rev. E **55**, 1577.
Lord, G. J. , A. R. Champneys, and G. W. Hunt, 1997, Phil Trans Roy Soc. London A, **355** 2137.
Love, A. E. H., 1944)*A treatise on the Mathematical Theory of Elasticity* (Dover Publications, New York), Section 260.
Mansfield, E. H., 1964, *The Bending and Stretching of Plates*, (Pergamon, New York).
Marion, J. B. and S. T. Thornton, 1995, *Classical Dynamics of Particles and Systems* (Harcourt Brace, New York).
Matan K., R. Williams, T. A. Witten, and S. R. Nagel, 2002, Phys. Rev. Lett. **88**, 076101.
Matsuo, E. S. and T. Tanaka, 1992, Nature **358** 482.
Menon, N., 2005, private communication.
Millman, R. S., and G. D. Parker, 1977, *Elements of Differential Geometry*, (Prentice-Hall, New Jersey).
Mora, T., and A. Boudaoud, 2002, Europhysics Letters **59**, 41.
Nelson, D., 1989, *Statistical Mechanics of Membranes and Surfaces*, edited by D. Nelson, T. Piran, and S. Weinberg, (World Scientific, Singapore).
Ortiz, M., and G. Gioia, 1994, J. Mech. Phys. Solids **42**, 531.
Ott, E., 2002, *Chaos in Dynamical Systems, 2nd Edition*, (Cambridge University, Cambridge, England).
Pogorelov, A. V. 1960, as summarized in L. D. Landau and E. M. Lifshitz *Theory of Elasticity, 3rd edition* Section 15. (Pergamon, Oxford UK, 1986).
Pogorelov, A.V., 1988, *Bendings of surfaces and stability of shells*, translated from the Russian by J.R. Schulenberger (American Mathematical Society, Providence, R.I.)
Polchinski, J. G., 1998, *String theory* (Cambridge University Press, New York)
Press, W. H., B. P. Flannery, S. A. Teukolsky, W. T. Vetterling, 1992, *Numerical Recipes in C : The Art of Scientific Computing, 2nd Edition*, (Cambridge University, Cambridge, England)
Radzihovsky, L., and J. Toner, 1998, Phys. Rev. E **57**, 1832.
Ramaswamy, S., 2001, Advances In Physics **50**, 297.
Robey, H. F., T. S. Perry, R. I. Klein, J. O. Kane, J. A. Greenough, and T. R. Boehly, 2002, Phys. Rev. Lett. **89**, 085001.
Safran, S. A., 1994, *Statistical Thermodynamics of Surfaces, Interfaces, and Membranes*, (Addison-Wesley, Reading, Mass).
Scheidl, R., and H. Troger, 1987, Computers and Structures, **27**, 157.
Seung, H. S., and D. R. Nelson, 1988, Phys. Rev. A **38**, 1005.
Sharon E., B. Roman, M. Marder, G. S. Shin, and H. L Swinney, 2002, Nature **419**, 579.
Shin, Y. M., M. M. Hohman, M. P. Brenner, and G. C. Rutledge, 2001, Applied Physics Letters **78**, 1149.
Stanley, H. E., 1987, *Introduction to Phase Transitions and Critical Phenomena*, (Clarendon Press, Oxford, UK).
Sultan E. and Boudaoud A., 2006, Phys. Rev. Lett. **96**, 136103 .
Tanizawa, K., and K. Miura, 1978, Trans. Japan Soc. Aero. Space Sci. **20** 175.
Thompson, J. M. T. and G. W. Hunt, 1984, *Elastic Instability Phenomena*, (Wiley, Chichester UK).
Turcotte, D. L., and G. Schubert, 2001, *Geodynamics, 2nd Edition*, (Cambridge University, Cambridge, England).
Venkataramani, S. C., 2003 , unpublished.
Venkataramani, S. C., 2004, Nonlinearity **17**, 301.
Venkataramani, S. C., T. A. Witten, E. M. Kramer, and R. P. Geroch, 2000, J. Math. Phys. **41**, 5107.
Vicsek, T., 1992, *Fractal Growth Phenomena, 2nd Edition*, (World Scientific, Singapore)).
Vliegenthart, G. A., and G. Gompper, 2006, Nature Materials **5**, 216.
von Karman, T., 1956, *The Collected Works of Theodore von Karman*, (Butterworths Scientific, London, England) **1**, 176.
Witten, T. A., and H. Li, 1993, Europhysics Letters **23**, 51.
Wood, A. J., 2002, Physica A. **313** 83.
Xu, L., W. W. Zhang, and S. R. Nagel, 2005, Phys. Rev. Lett. **94**, 184505.

Appendix: ridge-to-vertex crossover

In this Appendix we calculate the distance scale from the vertex at which corrections to the asymptotic Föppl–von Karman equations become significant. We give the details, since they do not appear in the literature.

As noted in Section V, the crossover occurs at that value of $\epsilon \equiv \frac{1}{2} - x$ such that the subleading term in the Föppl–von Karman equations become comparable with the leading term that gives Eq. 35. The subleading terms occur in the rescaling of Δ^2 given in Eq. 34. Since the subleading terms enter similarly in the force Föppl–von Karman equation and the geometric one, we consider only the force Föppl–von Karman equation. Defining $\xi \equiv \tilde{y}/q$ and using the form $\tilde{f} = q(\epsilon)p(\xi)$, the asymptotic force Föppl–von Karman equation is

$$\partial_{\tilde{y}}^4 \tilde{f} \sim q^{-3} p''''(\xi), \tag{40}$$

The leading correction is the term in $\lambda^{2\beta}$ in Eq. 34. This can be written as

$$\partial_x{}^2 \left[\partial_{\tilde{y}}{}^2 \tilde{f} \right]. \tag{41}$$

The factor in [...] is $q^{-1}p''(\xi)$. For $\epsilon \ll 1$, the scale factor $q(\epsilon) \sim \epsilon^{2/3}$. The reduced function $p(\xi)$ is even about $\tilde{y} = 0$. Performing the first derivative, one obtains

$$\partial_x \left[q^{-1} p''(\xi) \right] = \frac{q'}{q^2}(-p'' - \xi p'''). \tag{42}$$

We denote the ξ-dependent function in (...) as $p_3(\xi)$. Performing the second derivative, we find,

$$\begin{aligned} \partial_x{}^2 \left[q^{-1} p''(\xi) \right] &= \partial_x \left[\frac{q'}{q^2} p_3 \right] = q' \partial_q \left[\frac{q'}{q^2} p_3 \right] \\ &= q' \partial_q \left[\frac{q'}{q^2} \right] p_3 + q' \frac{q'}{q^2} \partial_q p_3 \\ &= q' \partial_q \left[\frac{q'}{q^2} \right] p_3 + q' \left[\frac{q'}{q^2} \right] \left[\frac{-q'}{q^2} \right] p_3{}'. \end{aligned} \tag{43}$$

Since q is a simple power of ϵ, we can write $q' = c\ q/\epsilon$, where c is a numerical constant. Using this fact, we may simplify further:

$$\partial_x{}^2 \left[q^{-1} p''(\xi) \right] = \frac{1}{q\epsilon^2} \left(a_1\ p_3 + a_2\ p_3{}' \right) \tag{44}$$

where a_1 and a_2 are numerical constants. The quantity in (...) is a function only of $\xi \equiv \tilde{y}/q$. We denote it as $p_4(\xi)$. It remains finite as $\epsilon \to 0$.

We may now compare the asymptotically dominant term of Eq. 1 with the leading correction. The condition that these two terms be comparable is:

$$\lambda^{4\beta} q^{-3} p'''' \simeq \frac{\lambda^{2\beta}}{q\epsilon^2} p_4. \tag{45}$$

Recalling that $\beta = -1/3$, that $q \sim \epsilon^{2/3}$, that $\lambda \sim h/X$ and that p'''' and p_4 are independent of ϵ, we conclude

$$(h/X)^{2/3} \sim \epsilon^{2/3} \tag{46}$$

or $\epsilon \sim h/X$, as announced in the text.